Preparation and Characterization of Cross-Linked Polymeric Nanoparticles for Enhanced Oil Recovery Applications

Nodar Al-Manasir

Supervisors

Bo Nyström

Anna-Lena Kjøniksen

DEPARTMENT OF CHEMISTRY

Acknowledgement

I would like to express my sincere thanks to my employer, Det Norske Veritas Petroleum Services for providing me with this scholarship from DNV Education Fund.

My expression of appreciations is to my supervisors Professor Dr. Bo Nyström and Dr. Anna-Lena Kjøniksen for their guidance and inspiration throughout this study. Having the honour of attending in two conferences Fefor 2008, and Mexico 2009. Bo, thank you for your active help, advice, support, encouragement, and valuable ideas and discussions. Anna-Lena; your door was always open for discussions, suggestions, technical problems, or just for talking, I really feel that you are more like a friend than a supervisor.

Many thanks to Dr. Kenneth Knudsen for making a new program for our spectrophotometer, and to Dr. Kaizheng Zhu who had prepared the PNIPAAM microgels.

I would like to thank Göran Karlsson for carrying out the cryo-TEM measurement.

My heartfelt thanks go to Ramón, and Atoosa for all help I got. Many thanks to all members in the polymer group at the University of Oslo for sharing knowledge and joys. I am also thankful to Amr M. Feteha for taking time to look at my Arabic abstract, and making some comments on it.

I am grateful to Prof. Dr. Hanne Grete Thomassen, Kjersti Kleveland, and Vidar Berget for their support through my life.

I owe a debt of gratitude to my sister Khoulod and her husband Isam for everything they have done for me.

A special thank to my dear parents, sisters, my brother, and parents-in-law for themes love and support through this demanding studium.
"Un doveroso e speciale ringraziamento ai miei cari suoceri per il loro dimostrato amore e appoggio durante questo mio impegnativo cammino istruttivo."

Last but not least, a big thanks to my beloved husband for sympathetic listening to my problems during the time of my seemingly endless studies, and for always being loving and supportive. You really were a strong support for this success. Finally a big kiss and thanks to my wonderful daughter Sara.

Nodar Al-Manasir

Oslo, March 2009

Table of Contents

List of Symbols and Abbreviations

AA	Acrylic Acid
AFFFF	Asymmetric Flow Field-Flow Fractionation
APS	Ammonium Persulfate
A_f	Amplitude of the Fast Relaxation Mode
A_s	Amplitude of the Slow Relaxation Mode
B	Empirical Factor
BIS	N, N`-methylenebisacrylamide
CMC	Critical Micelle Concentration
CP	Cloud Point
DLS	Dynamic Light Scattering
D_m	Mutual Diffusion Coefficient
DVS	Divinyl Sulfone
EHEC	Ethyl(hydroxyl ethyl)cellulose
EOR	Enhanced Oil Recovery
$g^1(q,t)$	First Order Electric Field Correlation Function
$g^2(q,t)$	Measured Homodyne Intensity Autocorrelation Function
HEC	Hydroxyethylcellulose
ILS	Intensity Light Scattering
I_t	Transmitted Light Intensity
I_0	Incident Light Intensity
K_B	Boltzmann Constant
L	Light Path Length of the Cuvette in Turbidimeter
LCST	Lower Critical Solution Temperature
LS	Light Scattering

M_n	Number Average Molecular Weight
M_w	Weight Average Molecular Weight
n	Refractive Index
PNIPAAM	Poly(N-isopropylacrylamide)
PNIPAAM-co-PAA	Poly(N-isopropylacrylamide-co-acrylic acid)
q	Wave Vector
q^{-1}	Length Scale
Rheo-SALA	Rheo-Small-Angle Light Scattering
R_g	Radius of Gyration
R_h	Hydrodynamic Radius
$R_{h,f}$	Fast Hydrodynamic Radius
$R_{h,s}$	Slow Hydrodynamic Radius
SDS	Sodium Dodecyl Sulfate
wt %	Weight Percentage
β	Stretched Exponent
Γ	Gamma Function
γ	Stretched Exponent
θ	Scattering Angle
λ	Wave Length of the Light
τ	Turbidity
τ_f	Fast Relaxation Time
τ_{fe}	Effective Fast Relaxation Time
τ_s	Slow Relaxation Time
τ_{se}	Effective Slow Relaxation Time

ABSTRACT

In this study, we will try to develop different microgel systems for enhanced oil recovery applications. The usage of microgels for this application has not been much studied, but it seems to have a great potential. The discussion regarding these systems has been subdivided into two parts. In the first part, chemically cross-linked nanoparticles from dilute aqueous alkali solutions of hydroxyethylcellulose (HEC) in the presence of a cross-linker agent (divinyl sulfone, DVS) have been examined. These nanoparticles were prepared from a reaction mixture, which was exposed to different stirring speeds during the cross-linking process. At various stages during the cross-linking procedure, the reaction was terminated and the species were characterized by means of turbidimetry, asymmetric flow field-flow fractionation (AFFFF), dynamic light scattering (DLS), and rheo-small-angle light scattering (Rheo-SALS) methods. During the cross-linking of a dilute polymer solutions, there is a constant competition between intrapolymer and interpolymer cross-linking. The DLS results show that intrachain cross-linking with contraction of the complexes is promoted and the growth of aggregates is inhibited by high stirring speed. The results from the Rheo-SALS measurements disclosed that at early stages during the cross-linker reaction, the complexes are fragile against shear forces, especially if the reaction mixture had been subjected to low stirring speeds. At a later state of cross-linking, more cross-links lead to a better stability of the species. The strategy discussed in this study is of special interest for enhancing the oil recovery applications, since the size and polydispersity of the particles can be tuned by changing the stirring speed and quenching time.

In the second part, uncharged chemically cross-linked poly(*N*-isopropylacrylamide) (PNIPAAM) microgels and charged PNIPAAM microgels with different amount of acrylic acid groups (PNIPAAM-*co*-PAA) were synthesized and the temperature-induced aggregation behavior of aqueous suspensions of these microgels were explored with the aid of dynamic light scattering (DLS), and turbidimetry. The DLS results show that the particles at all conditions would shrink at temperatures below the lower critical solution temperature (LCST). For the uncharged particles, the relative contraction effect is larger than what is observed for charged particles. The compression of the microgels cannot be traced from the turbidity results, but rather the values of the turbidity increase in the whole temperature interval. This phenomenon is discussed in the framework of a theoretical model. In a very dilute suspension, the size of the uncharged microgels is unaffected by temperatures above LCST. In this temperature range, uncharged particles of higher concentration and particles containing acrylic acid groups at low pH (pH = 2) aggregate, and macroscopic phase separation is approached at higher temperatures. The charged particles (pH = 7 and pH = 11) continue to collapse with increasing temperature over the entire temperature domain. The addition of an anionic surfactant such as SDS to the uncharged particles has been studied. This adsorption of the anionic SDS may endow a polyelectrolyte character of the uncharged polymer and will stabilize those against aggregation. This study demonstrates how the stabilization of microgels can be affected by factors such as polymer concentration, addition of ionic surfactant to uncharged particles, the amount of charged groups in the polymer, and/ or pH.

ABSTRACT (Arabic)

الملخص

في هذا البحث، سنحاول إكتشاف أنظمة مختلفة من الميكروجيل لتحسين طرق إستخلاص النفط الخام. إن إستخدام الميكروجيل في هذه الطرق لم يحظى بقدر واف من البحث، ولكنه يعد بإمكانات مغرية. تنقسم الدراسة في هذا البحث إلى قسمين. في القسم الأول سيتم بحث تصلب الروابط كيميائيا[1] لجزيئات النانو من المحاليل القاعدية المخففة مائيا للهيدروكسى إثيل سليلوز (HEC)[2] في مناخ يتوافر به عامل تصلب الروابط[3] ثنائي فينيل اوداي سيلفون (DVS)[4]. وقد تم إعداد جزيئات النانو هذه من مخلوط تفاعلي تحت سرعات مختلفة للتقليب خلال عملية تصلب الروابط. في مراحل مختلفة من عملية تصلب الروابط ، تم إيقاف هذا التفاعل وتم تصنيف الجزيئات طبقا لصفاتها بأنظمة تشمل جهاز قياس التعكير[5]، وجهاز التدفق المتناظر الحقلي التجزيئي[6] (AFFFF)، وجهاز التشتت الضوئي الديناميكي[7] (DLS) ، وجهاز التشتت الضوئي ذو الزوايا المنخفضة[8] (Rheo-SALS). خلال عملية تصلب الروابط لمحاليل البوليمر المخففه، لوحظ تنافس البوليمرات المحدودة والشاملة بإستمرار. أظهرت نتائج جهاز التشتت الضوئي الديناميكي (DLS), أنه تصلب الروابط السلسلي المحدود مع انكماش التجمعات كان معززا، وأن نمو هذه التجمعات كان مكبت في السرعات العالية للتقليب. كما أظهرت نتائج جهاز التشتت الضوئي ذو الزوايا المنخفضة (Rheo-SALS) أنه في المراحل الأولية خلال تفاعل تصلب الروابط, أن التجمعات كانت هشة تحت قوى الضغط خاصة أذا كان خليط التفاعل واقعا تحت السرعات البطيئة. بينما في المراحل المتأخرة لتصلب الروابطي, أدت زيادة تصلب الروابط إلى معدل إستقرار أفضل للجزيئات. أن موضوع هذا البحث ذو أهمية خاصة لتحسين طرق إستخلاص النفط الخام من الأبار, بما إن الحجم والتشتت المتعدد[9] لهذه الجزيئات يمكن تغيره من خلال تغير سرعه التقلب وأوقات الآخماد.

---

1) Chemically cross-linked
2) Hydroxyethylcellulose (HEC)
3) Cross-linker agent
4) Divinyl sulfone (DVS)
5) Turbidimetry
6) Asymmetric flow field-flow fractionation (AFFFF)
7) Dynamic light scattering (DLS)
8) Rheo-small-angle light scattering (Rheo-SALS)
9) Polydispersity

في القسم الثاني من البحث، تم إعداد جزيئات الميكروجيل غير المشحونة والمتصلبة الروابط كيميائيا بولي(ن-ايسوبروبيل الإكريلايد)[10](PNIPAAM) و جزيئات مشحونة منها بكميات مختلفة من مجموعات حمض الأكريلك[11] (PNIPAAM-co-PAA) ودراسه سلوك الحث الحراري لتجمعات المائيه لهذه الميكروجيلات بمساعدة جهاز التشتت الضوئي الديناميكي (DLS)، وجهاز قياس التعكير. حيث أظهر جهاز التشتت الضوئي الديناميكي(DLS) أن الجزيئات تقلصت في كل الاحوال في درجات الحرارة الأدنى من درجة الحرارة الحدية الدنيا للمحلول[12] (LCST). بالنسبة للجزيئات غير المشحونة، أظهر البحث أن الأثر النسبي للتقلص كان أعلى من الجزيئات المشحونة. كما أنه لا يمكن إقتفاء عملية تقلص جزيئات الميكروجيل من خلال نتائج جهاز التعكير ولكن يمكن تحديد قيم زيادة التعكر في حدود ثابتة لدرجات الحرارة. وقد تم بحث هذه الظاهرة في إطار نموذج نظري. في التركيبات المخففة جدا, لم تتأثر حجم جزيئات الميكروجيل غير المشحونة بدرجات الحرارة الاعلى من درجة الحرارة الحدية الدنيا(LCST) للمحلول. في هذه الحدود من درجات الحرارة، تم التوصل الى أن الجزيئات غير المشحونة ذات التركيز الأعلى والجزيئات التى تحتوي على مركبات حمض الأكريلك المتواجده في مناخ حمضي منخفض(pH=2) تتجمع, وتقترب من مرحلة الفصل الميكرسكوبي. بينما استمرت الجزيئات المشحونة في المناخ المتعادل و القاعدي (pH=7, pH=11) بلأنكماش مع إستمرار إرتفاع درجات الحرارة بدرجة أعلى من درجة حرارة المجال. كما تم دراسه الجزيئات غير المشحونة تحت أضافة عامل الفعاليه السطحي الايوني مثل دو ديسيل كبريتات الصوديوم[13] (SDS). أن هذا الامتصاص الكيميائي لعامل الفعاليه السطحي الايوني (SDS) يمنح جزيئات الميكروجيل الغير المشحونة خصائص أيونيه وبذالك يوازنها ضد التجمع. يظهر هذا البحث كيفية تأثر إستقرار الميكروجيل بعوامل مثل تركيز البوليمر، إضافة عامل الفعاليه السطحي الايوني للجزيئات غير المشحونة، كمية المجموعات المشحونة في البوليمر ودرجة الحموضة.

10) Poly (N-isopropylacrylamide) (PNIPAAM)
11) Poly (N-isopropylacrylamide-co-poly acrylic acid) (PNIPAAM-co-PAA)
12) Lower critical solution temperature (LCST)
13) Sodium dodecyl sulfate (SDS)

I. INTRODUCTION

I.1 Enhanced Oil Recovery

Unstable oil prices and increasing oil demand is a fact of life, even though a global peak of conventional oil production was expected to decay, energy insufficiency is one of the most important problems that faces humanity [1-4]. Liquid fuel prices will probably increase as a consequence of the decreasing production of cheap, easy-to-access oil. Without a practical solution, the economic, environmental, social, and political costs will be unprecedented with the opportunities of discovering new reservoirs decreasing [4,5], enhanced oil recovery (EOR) has become an important option to moderate shortage of oil production in reservoirs after they reach their peak production [3,4].

EOR processes often involve the injection of materials not normally present in the reservoir (polymers, foams, surfactants, solvents, etc.). They are categorized as thermal, chemical, or solvent methods. Polymer flooding is a chemical EOR process that has been studied since the late 1950s, and its application has become common since 1980 [6]. The basic process is consisting of using water soluble polymers of high molecular weight as water-flooding additives to control fluid movement in reservoirs, in order to improve sweep efficiencies, and to increase oil production. In most cases, polymer flooding is implemented as a tertiary process near the end of a water flood. In the oil fields, polyacrylamides and polysaccharides are the most commonly used water-based polymers [7-10]. Water-based polymers can also be injected with a cross-linking agent into the reservoir formation, and in this case a polymer gel is formed by the reaction between the polymer solution and a cross linking agent [7, 11]. In such practice a solution containing the polymer and cross-linker, is injected in desired zones and allowed sufficient time to set into a gel. In recent years, these gels are not only used in injection wells to divert the flow and shut off the flow of water in oil

production wells, but also used more substantially as agents in enhanced polymer flooding [12,13]. The main disadvantages of EOR using linear polymer solutions compared with cross-linked polymer solutions are plugging after a given time [14], mechanical and chemical degradation [15,16] and less stability with respect to high temperatures and salinity [17].

In this project, we aim to find new, low cost microgels that can be used in enhanced oil recovery (EOR) applications without any adverse effects on the environment.

I.2 Polymers

A polymer is a large molecule that is made of small constituent parts (monomers) linked to each other [18]. The behavior of polymers in an aqueous environment depend on a number of factors, in particular various, intramolecular and intermolecular interactions such as van der Waales forces, electrostatic interactions, hydrophobic associating, and hydrogen bonds. For example, if the polymer contains electric charges, the polymer tends to expand due to intramolecular electrostatic repulsive interactions, charges also have consequences for the sensitivity of the polymer solution to electrolyte concentration and pH. Hydrophobic interactions and hydrogen bonds often result in an effective polymer-polymer attraction, which tends to both contract the polymer molecules and cause interpolymer associating [19]. Some polymers respond to change of physical or chemical stimuli, such as temperature, electric and magnetic field, solvent, mechanical stress, radiation (UV, visible light), and ionic strength [20]. Polymers can be divided into biopolymers and/ or synthetic polymers.

Biopolymers are classified as macromolecules which are produced by living organisms. Some examples of this kind of biopolymers are proteins, peptides, DNA, cellulose, cellulose derivatives and other polysaccharides. They are responsible for the biological functions of molecular sensing, catalysis, molecular motions and homeostatsis [20].

Synthetic polymers are classified as macromolecular compounds which are chemically manufactured from separate materials by human intervention. Poly (N-isopropylacrylamid) (PNIPAAM), polyethylene glycol (PEG), polystyrene (PS), polyethylene (PE), polyvinyl chloride (PVC), polypropylene (PP), nylon, and polyacrylamide (PAAM) are some examples of this type of polymers.

I.3 Gels

A polymer gel is a polymeric material that has both solid and liquid-like properties. Gels are mostly liquid in composition with respect to weight and volume, while their structure is a solid like.

Hydrogels are defined as aqueous cross-linked polymers that exhibit viscoelastic or pure elastic behavior. One of their most important features is their swelling capacity; they can absorb water up to one thousand times more than their dry weight [21-23]. Some hydrogels exhibit a stimuli responsive behavior [24,25]. They are widely used in many applications such as hygiene, cosmetics, agriculture, medicine, biotechnology, and petroleum recovery treatments of mature reservoirs because of their unique characteristics like hydrophilicity, swelling in aqueous media, and non-soluble nature in aqueous fluids [26-30]. Hydrogels can be classified in different ways but in this work we will concentrate mostly on the classification based on the cross-links type. Cross-links are important to maintain the 'network' structure of the hydrogels and to prevent dissolution of the hydrophilic chains [31]. Based on the type of cross-links there are two classes of hydrogels.

- Physically Cross-linked Hydrogels:

These hydrogels are cross-linked by physical forces such as hydrophobic interactions, hydrogen bonds, electrostatic forces, etc. Some hydrogels in this class can go from a three-dimensionally stable gel structure to the polymer solution, and do this reversibly, by changing external variable such as the temperature, concentration, pH, ionic strength, etc. [32]. An example of this kind of hydrogel is poly(acrylic acid) and poly(methacrylic acid) forming hydrogen bonds with (ethylene glycol), which results in the formation of hydrogels [33,34]. Another example is ethyl(hydroxyl ethyl)cellulose (EHEC) in the presence of an ionic surfactant. This system form thermoreversible gels at elevated temperatures [31,35,36].

- Chemically Cross-linked Hydrogels:

When a suitable cross-linker is added to an aqueous polymer solution, the polymer molecules are cross linked by covalent chemical bonds, and a permanent three-dimensional network is formed. This type of chemically hydrogels is more stable than the physically cross-linked hydrogels because the cross-links are formed by covalent bonds [31]. Usually they have a permanaent structure. An example of this kind of hydrogel is hydroxyethylcellulose (HEC) in the presence of the difunctional cross-linker divinyl sulfone (DVS) [37-39].

Microgels are colloidally stable hydrogel particles. Their size ranges typically from 50 nm to 5 μm [40]. Microgels possesses several advantages over bulk gels due to smaller size and volume, higher surface area, faster response to stimuli, and higher diffusivity [41]. Unusual properties of microgels lead to various applications such as drug delivery [42-44], biosensing [45,46], chemical separations [47,48], catalysis [49,50], optics [51,52], and EOR [39,53]. Many methods have been developed for preparing microgels, including emulsion polymerization, inverse microemulsion polymerization, anionic copolymerization, and cross-linking of neighboring polymer chains [40,54-61].

I.4 Polymer-Surfactant Interactions

During the last years, the synergism of surfactants and polymers in aqueous solution has attracted much interest in fundamental and applied research. The interest of this topic is driven by the numerous industrial applications of water-borne fluids incorporating mixtures of polymers and surfactants. This type of systems is found in fluids for enhanced oil recovery, paints, food preparations, cosmetic formulations, and pharmaceutical compositions [36]. It is well established that the interaction of a non-ionic polymer such as (PNIPAAM) with an anionic surfactant such as sodium dodecyl sulphate (SDS) can induce charging effects of the polymer and in effect imparting polyelectrolyte properties to the non-ionic polymer [62]. The strong polymer-surfactant interactions often manifest themselves through a significant viscosity enhancement at a certain concentration of the surfactant [36,63-68].

Addition of surfactant alters the thermodynamic conditions in a solution and the cloud point temperature can be effected [69]. Surfactants adsorb onto amphiphilic polymers and form polymer-surfactant complexes. As an example, adsorption of ionic surfactants onto a polymer adds both hydrophobic groups and charged groups to the polymer-surfactant complex. The ionic groups favour dissolution and the hydrophobic group favour aggregation. Depending on the amount and nature of adsorbed surfactant, the polymer-surfactant complex can experience improved or worsened thermodynamic conditions [69]. For many polymer/surfactant systems, the viscosity goes through a maximum as the surfactant concentration is increased [70-72]. For PNIPAAM, addition of a small amount of an anionic surfactant leads to poorer thermodynamic conditions. This results in a cloud point depression. At a higher surfactant concentration, the thermodynamic conditions are improved and the cloud point increases.

II. BACKGROUND

II.1 Materials

II.1.1 Hydroxyethylcellulose

Figure 1: *HEC is white or yellowish powder.*

Hydroxyethylcellulose (HEC) is a hydrophilic non-ionic polymer, which is usually sold as a white or yellowish powder, see Figure 1. HEC has antibacterial properties and can be classified as an environmentally friendly biopolymer. It is prepared by the reaction of purified cellulose with ethylene oxide, usually in the presence of a base such as sodium hydroxide. The base activates the cellulose matrix, in combination with water, by disrupting hydrogen-bonded crystalline domains, thereby increases the accessibility to the alkylating reagent. The activated matrix is usually termed alkali cellulose. The base also promotes the etherification reaction. Reactions are typically conducted at elevated temperature, and under nitrogen to inhibit oxidative molecular weight degradation of the polymer [73].The typical overall reaction for the production of HEC can be written as follows.

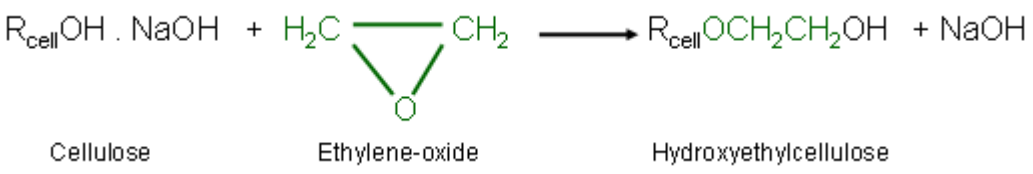

The chemical structure of HEC is given in Figure 2. HEC is used in various industrial fields such as coating, cements, thickeners, pharmaceuticals, oil-well fracturing, drilling applications, cosmetic, inks, papers, lubricants, gels, and agricultural formulations. HEC is not degraded by common bacteria [74].

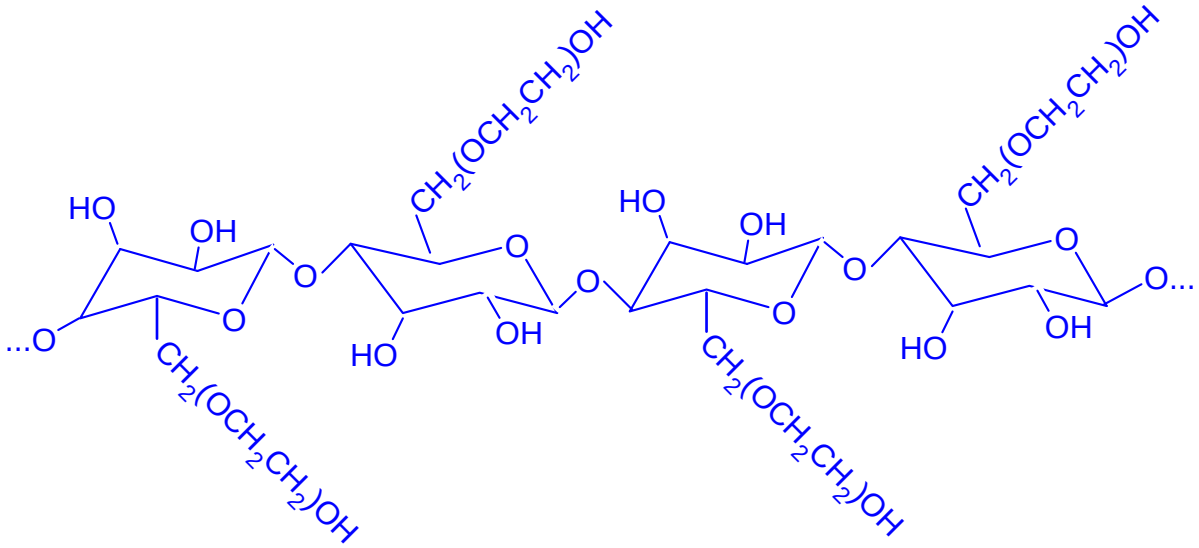

Figure 2: *An illustration of the HEC structure.*

II.1.2 Divinyl Sulfone

Divinyl sulfone (DVS) has been widely used to cross-link hydroxyl containing polymers to prepare hydrogels [75], microgels [39,62,76] and nanoparticle networks [77] in alkaline solutions (around pH ≈ 12 or higher) [78]. The advantage of using DVS as a cross-linker is the possibility of assessing the extent of the incorporation of the DVS by sulfur microanalyses [78]. The chemical structure of DVS is illustrated in Figure 3.

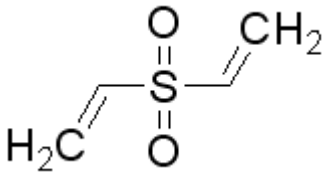

Figure 3: *The chemical structure of DVS.*

The reaction between a polymer containing hydroxyl groups and a cross-linking DVS is illustrated in Figure 4. This figure demonstrates how the cross-linker operates in connecting polymer chains containing hydroxyl functional groups. It is observed that this kind of reaction has to be done under basic conditions. The free hydroxyl groups on the polymer chain can react with the hydroxyl ions in the solvent and form poly-O^- anions at alkaline conditions. Sulfone is an electron-drawing group. According to the chemical structure of DVS, the terminal carbon atom is electron deficient, and has a positive charge to some extent. This will enable the terminal carbon atom to be attacked by the poly-O^- groups follow-on a Michael addition reaction. In principle this kind of reaction should not generated any byproduct, but in practice DVS is hydrolyzed by water (slowly at neutral pH and more rapidly in alkaline solution) [78].

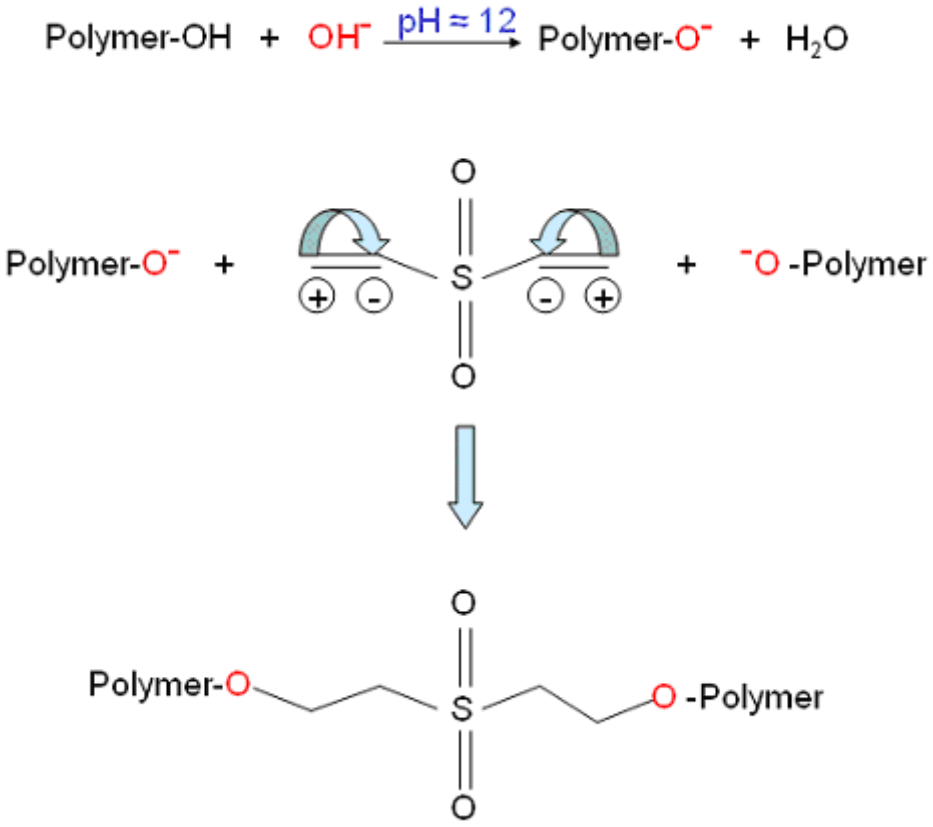

Figure 4: *Reaction scheme for cross-linking of hydroxyl-functional polymers with DVS.*

II.1.3 Cross-Linked acrylamide-based polymer gels

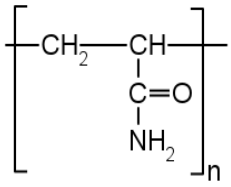

Figure 5: *Chemical structure of polyacrylamide.*

Polyacrylamide (PAAM) is a cost effective polymer, with the chemical structure shown in Figure 5. It can be obtained in the form of either a powder or an aqueous solution. The first study of cross-linked acrylamide gels was made in the late 1950s, as reported by White in 1960 [79]. White's work shows that the swelling degree of acrylamide (AAM) cross-linked with N,N'-methylenebisacrylamide (BIS) decreases with increasing crosslinking density [79,80]. The volume transition of polyacrylamide gels has been widely studied since 1984, and Hirokawa [81] found that non-ionic N-isopropylacrylamide polymer gels shrink when the temperature is increased. PAM-based polymer gels or stimuli-responsive microgels are frequently used in water treatment, paper manufacturing, mining/mineral processing, and the petroleum industry [82,83]. The vast array of applications of PAAM-microgels arise from their stimuli-responsive nature, that is, their ability to undergo reversible volume phase transitions in response to environmental stimuli such as pH [84,85], temperature [84], ionic strength [86], solvent [87], and the action of an external electromagnetic field [88], see Figure 6.

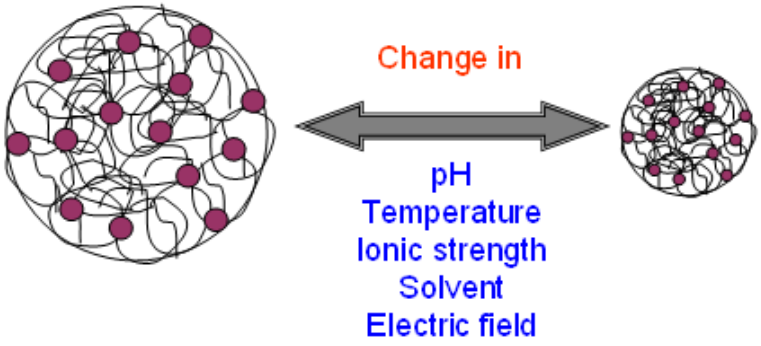

Figure 6: *Schematic illustration of change in microgel size in response to various environmental stimuli.*

One of the most studied classes of responsive polymers is the temperature sensitive poly(*N*-isopropylacrylamide) (PNIPAAM). PNIPAAM has been synthesized by a variety of techniques: redox initiation, free radical initiation, ionic initiation, and also using radiation [89].

When the solution temperature is raised above the lower critical solutions temperature (LCST for aqueous solutions of PNIPAAM is approximately 32 ^{o}C), this polymer undergoes thermally induced deswelling [89]. PNIPAAM is highly solvated, at temperatures well below the LCST, owing to hydrogen bonds between water molecules and amide residues of the polymer chains [89]. These hydrogen bonds are increasingly disrupted upon heating, causing water to act as a poorer solvent for PNIPAAM, thus leading to gradual chain collapse. Therefore, the hydrophobicity of the polymer is enhanced at elevated temperatures. This effect can easily lead to multichain association and the growth of huge aggregates.

As a result, heating of an aqueous suspension of chemically cross-linked PNIPAAM microgels can evoke a situation where intrachain contraction is overshadowed by interpolymer aggregation at high temperatures. The aim of the present investigation is to address this issue and to present strategies to control temperature-induced interpolymer aggregation.

II.1.4 Surfactants

Surfactants are low to moderate molecular weight compounds which contain a hydrophobic part, which is generally readily soluble in oil but with low water solubility, and a hydrophilic (or polar) part, with low oil solubility, but which is easily soluble in water [19], see Figure 7.

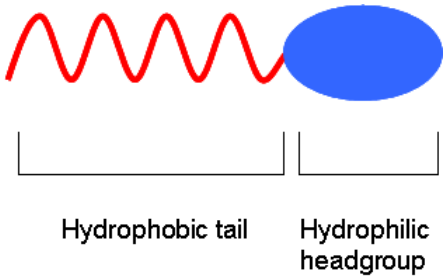

Figure 7: *Schematic illustration of a surfactant molecule.*

Surfactants are classified according to their hydrophilic headgroup, they can be either ionic or nonionic. The ability to self-associate into micellar structures when the surfactant concentration in the solution surpasses a limiting value is known as the critical micelle concentration (CMC) [19]. Surfactants are widely used as additives to modify the properties of polymeric systems for a variety of applications [90,91].

II.1.4.1 Sodium Dodecyl Sulfate

Sodium dedecyl sulfate (SDS) ($CH_3(CH_2)_{11}OSO_3Na$) is a common anionic surfactant, see Figure 8, with a CMC of about 8.0 m*M* in pure water solution at 25 °C [92-95].

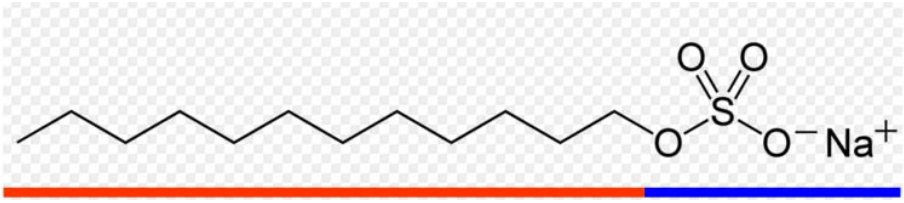

Figure 8: *Chemical structure of SDS.*

II.2 Experimental Methods

II.2.1 Mechanical Stirring

To apply various shear forces on the reaction mixtures, a mechanical stirrer device of the type IKA EUROSTAR power control-visc was purchased from IKA®-Werke Gmbh & Co. KG, Germany. A principal sketch of the experimental set-up with the mechanical stirrer is displayed in Figure 9.

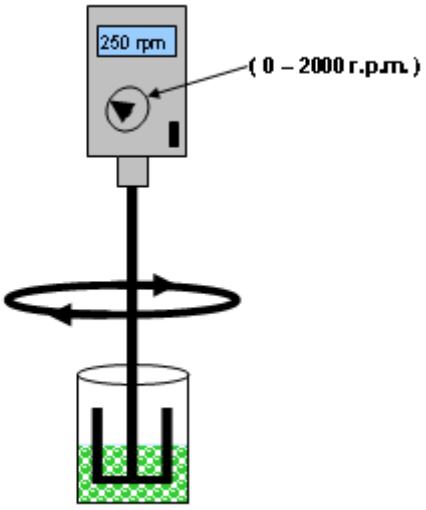

Figure 9: *Schematic demonstration of the mechanical stirring setup.*

II.2.2 Turbidity

Turbidity is a measure of the cloudiness of the samples and how much the solute hinders the passage of light. In this work, a spectrophotometer is used to determine the turbidity of the samples. This optical technique employs transmission measurements, in which the detector is optically in line with the light source, see Figure 10. Particles in the sample scatter and absorb the incoming light, and consequently less light is transmitted through the sample. The decrease in light intensity, compared to a cuvette containing the pure solvent is measured. The turbidity measurements give insight into structural changes of the systems on a global scale and also the thermodynamic and associative properties of polymer solutions. A steep increase in the turbidity of a polymer solution may be due to deteriorated thermodynamic conditions of the system.

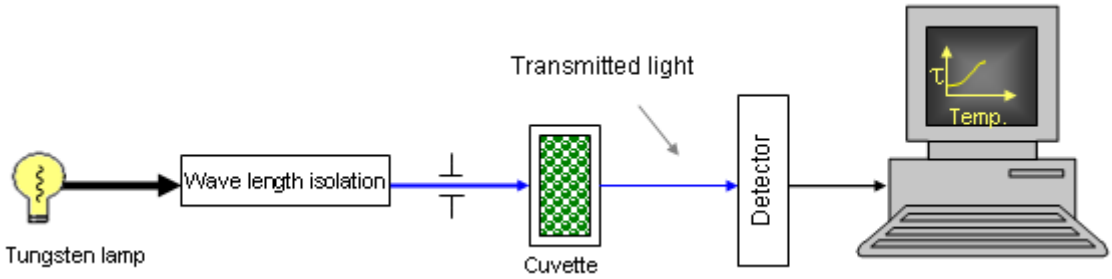

Figure 10: *Schematic illustration of turbidity measurements using a spectrophotometer.*

The spectrophotometer that has been used in this work is a computer-controlled Thermo Spectronic Helios Gamma with a good temperature control in the range (0-100°C). It is a single beam UV-Vis spectrophotometer with a wavelength range of 190-1100 nm and a fixed 2 nm bandwidth, and it can measure in two modes:

- Absorbance (how much light is absorbed by the sample).
- Transmittance (the percentage of the incoming light that goes through the sample)

To calculate the turbidity (τ) from the measured transmittance, the following expression is used:

$$\tau = (-1/L) \ln (I_t/I_0) \qquad (1)$$

Where: L is the light path length in the cuvette (1 cm)

I_t is the transmitted light intensity

I_0 is the incident light intensity

The cloud point (CP) of the samples can be determined from the turbidity curves, and is taken as the time of the initial steep increase in the turbidity.

II.2.3 Light Scattering (LS)

Light Scattering (LS) is a powerful technique for characterization of particles in solution. Intensity light scattering (ILS), and dynamic light scattering (DLS) are two different experimental methods, but the same instrument is used for both. Intensity- and dynamic light scattering give complementary information. By using ILS, the molecular weight (M_w), the radius of gyration (R_g), the fractal dimension (d_f), and the second virial coefficient (A_2) can be calculated. ILS is a well-established technique for determining size, shape, and structure. The hydrodynamic radius (R_h), diffusion coefficients (D), hydrodynamic correlation lenght ζ_h for semidilute samples, micellar size, and particle size distribution can be calculated from DLS experiments. For this reason they are commonly used to characterize polymer solutions [96-98].

In light scattering experiments, we probe the sample on a length scale of q^{-1}, where q is the wave vector defined as $\boldsymbol{q = 4\pi n \sin(\theta/2)/\lambda}$. Where λ is the wavelength of the incident light in a vacuum, θ is the scattering angle (i.e., the angle between the incoming and scattered light) and n is the refractive index of the medium. A principal sketch of the experimental set-up of the LS is displayed in Figure 11.

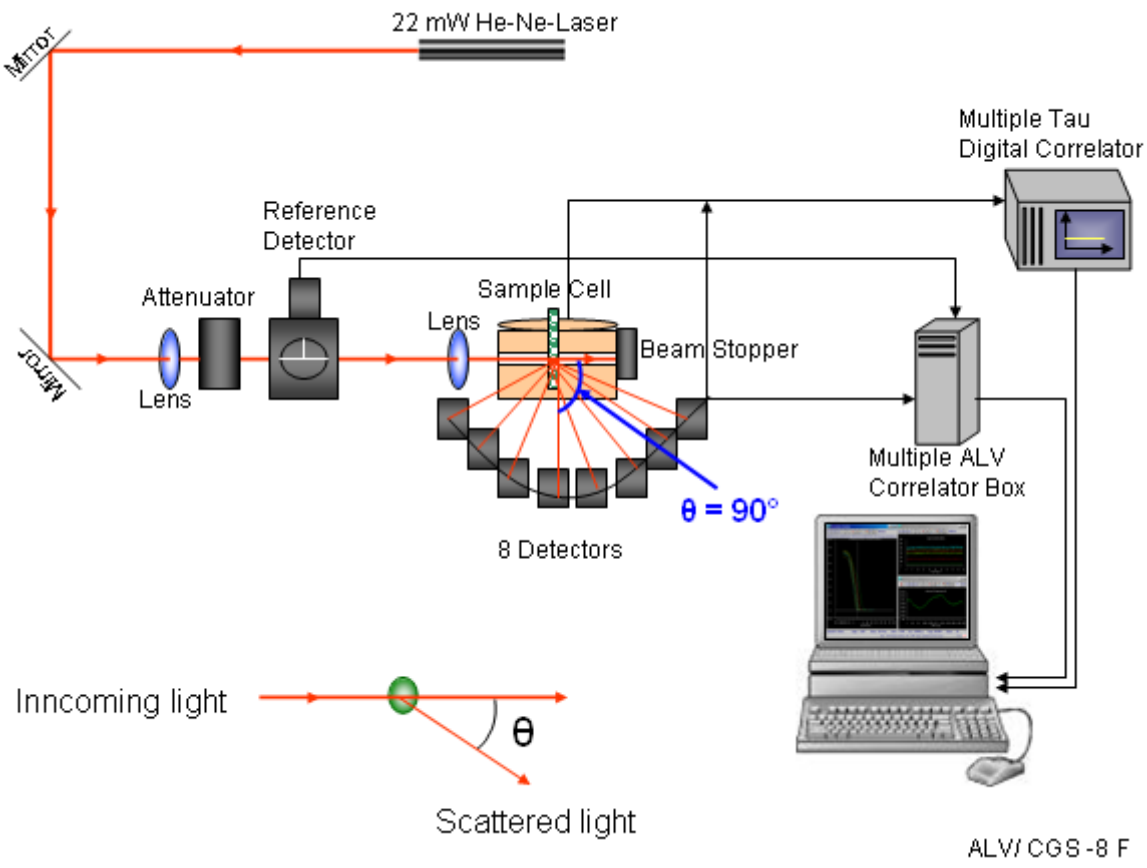

Figure 11: *Schematic illustration of the light scattering apparatus.*

ALV/CGS-8F is multi-detector version compact goniometer system, with 8 fiber-optical detection units, from ALV-GmbH., Langen, Germany. The beam from a Uniphase cylindrical 22 mW HeNe-laser, operating at a wavelength of 632.8 nm with vertically polarized light, was focused on the sample cell (10-mm NMR tubes, Wilmad Glass Co., of highest quality) through a temperature-controlled cylindrical quartz container (with 2 plane-parallel windows), vat (the temperature constancy being controlled to within ± 0.01 ^{o}C with a heating/cooling circulator), which is filled with a refractive index matching liquid (*cis*-decalin).

II.2.3.1 Dynamic Light Scattering (DLS)

Dynamic light scattering (DLS), which is also known as "photon correlation spectroscopy" or "quasi-elastic light scattering", is a well established technique used for characterizing dynamics, on different length and timescales, in systems of various complexity. This technique measures the time dependent fluctuations in the intensity of scattered light, which occurs because the particles are undergoing random, Brownian motion. This random motion of the particles (within the small measuring volume) causes a dynamic pattern of fluctuation in the scattered light arriving at the detector. These distortions in light are measured to calculate the ease of movement of particles in a liquid medium. As light scatters from the moving macromolecules, this motion imparts a randomness to the phase of the scattered light, such that when the scattered light from two or more particles is added together, there will be a changing destructive or constructive interference. This leads to time-dependent fluctuations in the intensity of the scattered light that can be measured over a time range from tenths of a microsecond to more than one hour. DLS measurements probe how concentration fluctuations relax toward equilibrium at a length scale of q^{-1}. The fluctuations are quantified via the second order correlation function:

$$g^2(t) = \frac{\langle I(t)I(t+\tau)\rangle}{\langle I(t)\rangle^2} \qquad (2)$$

Where $I(t)$ is the intensity of the scattered light at time t, τ is the time measured from the time t, and the brackets indicate averaging over all t. Analysis of these intensity fluctuations at different scattering angles enables the determination of the distribution of diffusion coefficients of the particles from which, the hydrodynamic radius of the particles can be calculated. The strength of this technique lays in its ability to examine samples containing

broad distributions of species of widely differing molecular masses and various sizes of aggregates [96-98].

II.2.3.1.1 Analysis of the Dynamic Light Scattering data

If the scattered field obeys Gaussian statistics (which most systems do, provided they are ergodic, and not very turbid), the experimentally determined homodyne intensity autocorrelation function, $\mathbf{g^2(q,t)}$, can be directly related to the theoretically amenable first-order electric field autocorrelation function, $\mathbf{g^1(q,t)}$, by the Siegert relation [99].

$$g^2(q,t) = 1 + B|\, g^1(q,t)\,|^2 \qquad (3)$$

Where B is usually treated as an empirical factor.

For suspensions containing particles with different size distribution, the nonexponential behavior of the autocorrelation function can be portrayed by using a Kohlrausch-Williams-Watts [100,101] stretched exponential function. This procedure has been reported [102-105] to be powerful in the analysis of correlation functions obtained from various colloid systems. This approach is also successful to describe the correlation function data in the second part of this work (PNIPAAM microgels), and the correlation functions are fitted with the aid of eq.4.

$$g^1(t) = \exp\left[-(t/\tau_{fe})^{\gamma}\right] \qquad (4)$$

Where τ_{fe} and γ are fitting parameters.

While the correlation functions for dilute or semidilute solutions of more complex systems can often be described by the sum of a single exponential flowed by a stretched exponential:

$$g^1(t) = A_f \exp\left[-t/\tau_f\right] + A_s \exp\left[-(t/\tau_{se})^\beta\right] \qquad (5)$$

With $A_f + A_s = 1$. The parameters A_f and A_s are the amplitudes for the fast and the slow relaxation time, respectively. The variables τ_f and τ_{se} are the relaxation times characterizing the fast and the slow relaxation process, respectively. This type of bimodal relaxation process has been reported [37,100,106] from DLS studies on aggregating polymer systems of various natures.

The variables τ_{fe} and τ_{se} are some effective relaxation times, and γ ($0 < \gamma \leq 1$) and β ($0 < \beta \leq 1$) measure the widths of the distributions of relaxation times. The mean relaxation time for the fast and slow mode is given by:

$$\tau_f = \frac{\tau_{fe}}{\gamma}\Gamma\left(\frac{1}{\gamma}\right) \qquad (6a)$$

$$\tau_s = \frac{\tau_{se}}{\beta}\Gamma\left(\frac{1}{\beta}\right) \qquad (6b)$$

Where Γ is the gamma function.

In the analysis of the correlation functions by means of either eq.4 or eq.5, a nonlinear fitting algorithm (a modified Levenberg-Marquardt method) was employed to obtain best-fit values of the parameters τ_{fe}, τ_{se}, A_f, γ, and β. The fast mode is diffusive (q^2-dependent) for all the samples and it yields the mutual diffusion coefficient D_m **($\tau_f^{-1} = D_m q^2$)** of molecularly dispersed species and small aggregates. The slow mode (the second term on the right-hand

side of eq.5) characterizes the dynamics of large aggregates and this mode is also always found to be diffusive.

When the relaxation modes are found to be diffusive, this enable us to calculate the hydrodynamic radii ($R_{h,f}$, and $R_{h,s}$) from the fast and slow relaxation times, respectively, via the Stokes-Einstein relationship.

$$R_h = \frac{k_B T}{6\pi\eta D} \qquad (7)$$

Where k_B is the Boltzmann constant, T is the absolute temperature, η is the solvent viscosity, and D is the diffusion coefficient of the species in the solution.

II.2.4 Rheo-Small Angle Light Scattering (Rheo-SALS)

Rheo-small angle light scattering (Rheo-SALS) is one of the most widely used techniques to obtain simultaneously determination of both structural and rheological information [107]. While pure rheology methods mainly provide information on the macroscopic behavior of the samples, information on the microstructure can also be simultaneously acquired via rheo-SALS measurements. This is often helpful for a better understanding of the rheological behavior. Simultaneous rheological and small angle light scattering experiments are conducted under the influence of a prescribed shear rate. The scattered light illuminates a semi-transparent screen, and is recorded by a camera. A schematic illustration of the Rheo-SALS setup utilized in this work is shown in Figure 12.

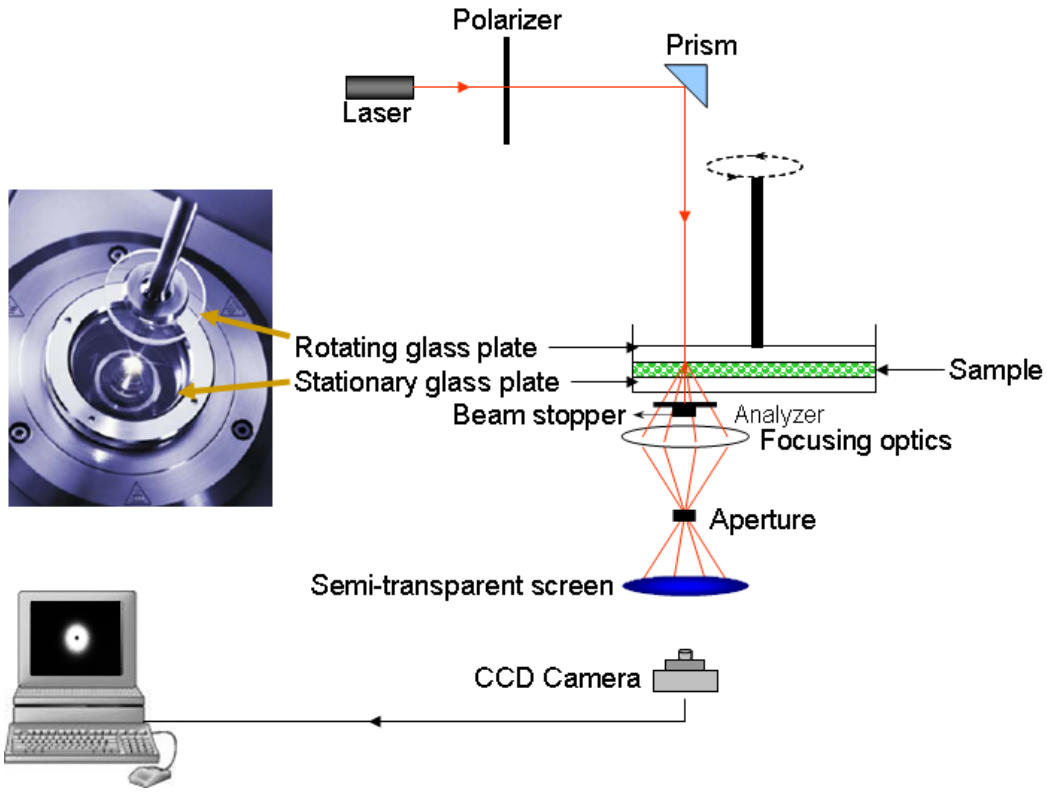

Figure 12: *Schematic illustration of the small angle light scattering apparatus.*

II.2.4.1 Analysis of Rheo-Small Angle Light Scattering data

In light scattering, the angular distribution of the scattered light, which is induced by an incoming primary laser beam, is measured and analyzed with respect to the scattering angle and intensity. Under certain assumptions, structural information can be obtained from the scattered light intensity distribution. 2D scattering patterns are captured at a given time using a CCD camera, and the data can be analyzed by the SALS software. A picture obtained direct from a Rheo-SALS measurement, and the same picture after it is converted by the software is illustrated in Figure 13.

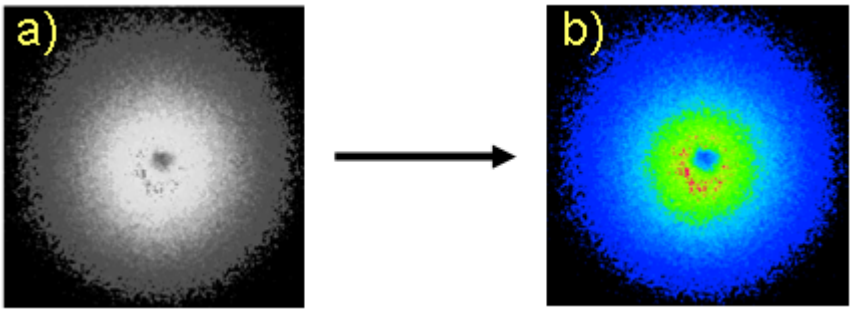

Figure 13: *a) A typical 2D scattering pattern. b) A typical picture after utilizing the SALS software.*

From the scattering pattern, an intuitive recognition of the scattering intensity can be obtained roughly by observing the colour of the pattern, which indicates a very intensive scattering (red, green) near the centre of the scattering circles, and a gradually decreased intensity (light- and dark blue) with decreasing scattering intensity. The low q-values are measured closest to the center, and as the distance to the center is increased, higher of q-values are obtained. The dependence of the intensity with shear rate can be also evaluated for a given q value.

II.2.5 Asymmetric Flow Field-Flow Fractionation

Asymmetric flow field-flow fractionation (AFFFF) is an innovative separation method for efficient separation and characterization of protein, polymer and nanoparticles in a fast and gentle way. Based on the diffusion rate of the sample, the separation occurs in flow channel. The instrument utilizes two detectors, a refractive index detector (RI) that detects the concentration of the sample, and a multi angle light scattering detector (MALS), which measures the molecular weight and size of the molecules. AFFFF offers the possibility to determine a broad variety of different physicochemical parameters of the sample [108], such as the number average molecular weight (M_n), weight average molecular weight (M_w), and radius of gyration (R_g). The instrument used in this study has a large separation range. Nanoparticles can be separated in the range of 1 nm to 100 µm and proteins, peptides and polymers with molecular weights from 10^3 to 10^{12} Da can be characterized. A principal sketch of the experimental set-up of the AFFFF is displayed in Figure 14.

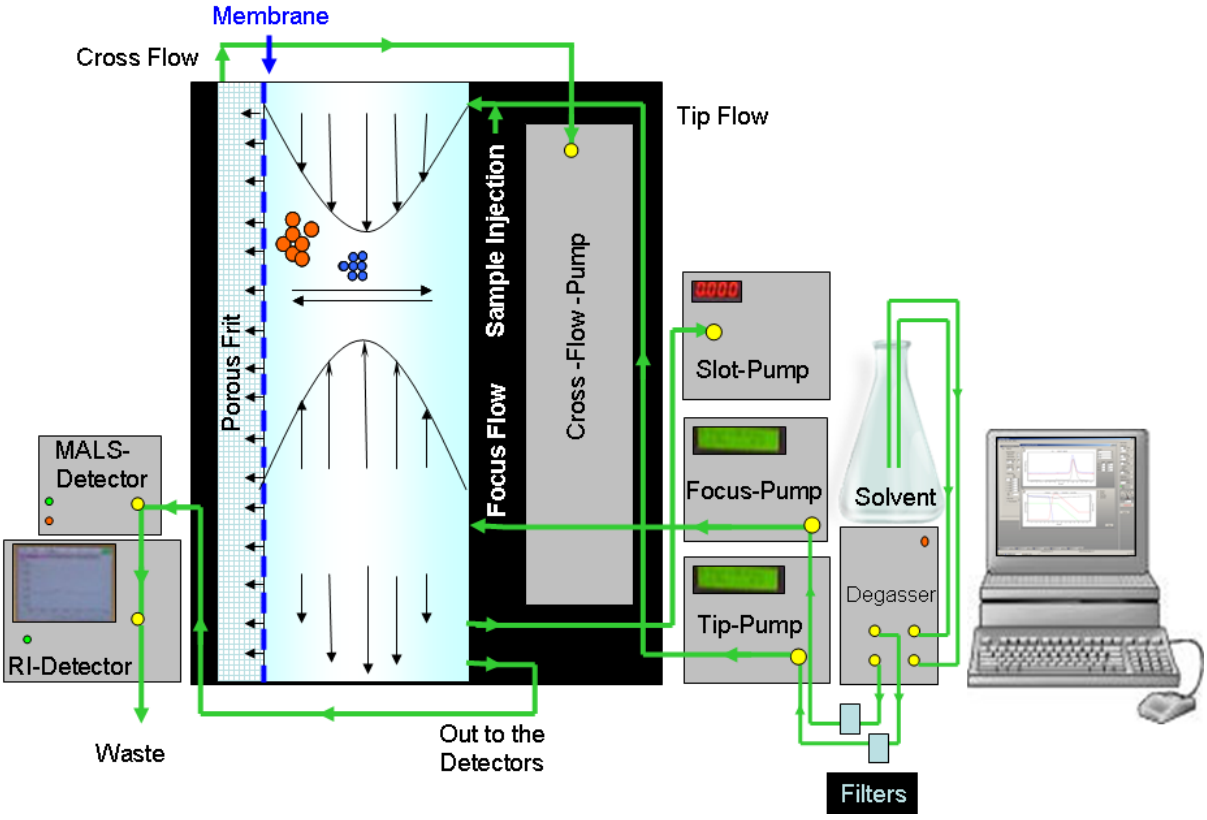

Figure 14: *Schematic illustration of the asymmetric flow field-flow fractionation apparatus.*

The sample is injected with the tip flow, and is focused into a narrow band by a parabolic flow profile from both sides. At the same time, the sample is submitted to a flow-field created by the cross flow, pressing the sample towards the membrane. The diffusion of the molecules causes large molecules to be located closest to the membrane, and smaller molecules are located further out from the membrane see Figure 14. After the focusing step, the focus flow is reduced to zero and then the cross flow is gradually reduced to zero causing the small molecules to be eluted first followed by larger molecules. During the measurement, the tip flow is varied in order to keep the detector flow constant (detector flow = tip flow + focus flow – cross flow – slot pump flow).

Many studies have been reported on the characterization of biomacromolecules such as polysaccharides with the aid of AFFFF [109-112]. However, it is important that a careful attention to correct operating conditions for each individual sample with different structural and chemical properties is observed [113].

II.2.5.1 Analysis of Asymmetric Flow Field-Flow Fractionation data

The weight –average molecular weight (M_w), number-average molecular weight (M_n), and radius of gyration (R_g) can be determined by using the Postnova software without standards (AF2000 control, version 1.1.011). Information about the molecular weight of the samples at different stages was obtained using this software with a Zimm fit.

II.2.6 Refractometer

The PTR 46 refractometer utilized in this study can measure the refractive index, n, of the samples in the range 1.32 – 1.68, with an accuracy of 0.0001 using a wavelength of 589 nm. The temperature is peltier-controlled in the range 15-40°C. By plotting the refractive index versus the temperature, the refractive index can be extrapolated to higher temperatures, see Figure 15.

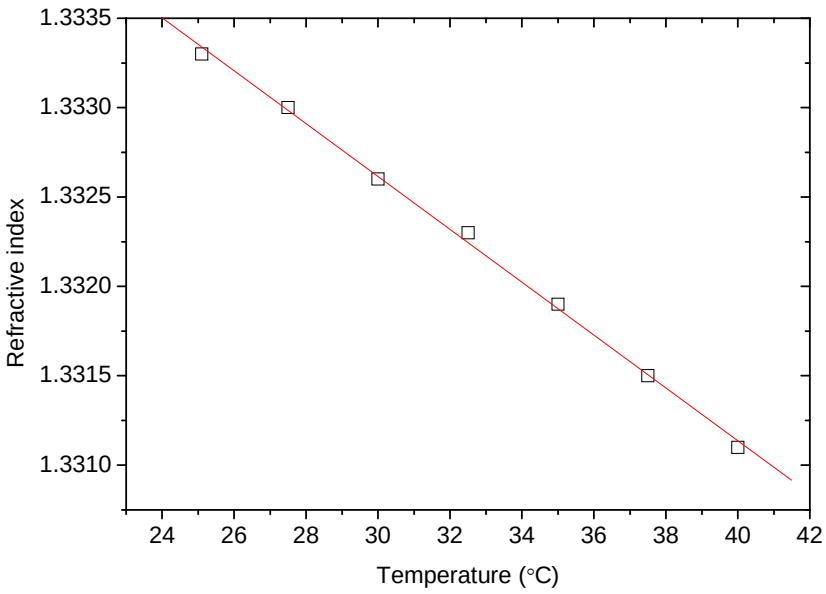

Figure 15: The refractive index as a function of the temperature for uncharged PNIPAAM at pH=2.

The line is a linear fit to the experimental data, and a refractive index value at T > 40 °C is extrapolated from this line.

III. EXPERIMENTAL SECTION

III.1 Materials and Solution Preparation

III.1.1 HEC cross-linked by DVS

In this work, we used a hydroxyethylcellulose (HEC) sample with the trade name Natrosol 250 GR (lot. no. A-0382) that was provided by Hercules, Aqualon Division. The degree of substitution of hydroxyethyl groups per repeating anhydroglucose unit of the polymer is 2.5 (given by the manufacturer). The weight-average molecular weight (M_w = 400 000) and the overlap concentration (c* = 0.25 wt %) of this HEC sample in aqueous solution have both been reported previously [37]. To remove salt and other low-molecular-weight impurities, dilute HEC solutions were dialyzed against Millipore water for 7 days and recovered by freeze drying. Regenerated cellulose with a molecular weight cutoff of ~ 8000 (Spectrum Medical Industries) was employed as dialyzing membrane. The cross-linking agent DVS was purchased from Merck and used without further purification.

All solutions were prepared by weighing the components and Millipore quality water was always used. After freeze-drying, HEC was redissolved in 0.05 M NaOH (pH ≈ 12; alkaline conditions are necessary for the cross-linker reaction to proceed) solution with a fixed polymer concentration of 0.1 wt % (this concentration is far below the overlap concentration), and the solution was homogenized by stirring at room temperature for 1 day. All experiments were carried out at 25^{o}C or room temperature.

III.1.2 PNIPAAM microgels

N-isopropylacrylamide (NIPAAM, Acros) was recrystallized from a toluene/hexane mixture solvent and dried at room temperature under vacuum prior to use. *N*,*N*′-methylenebis(acrylamide) (BIS), ammonium persulfate (APS), acrylic acid (AA), and sodium dodecyl sulfate (SDS) were utilized in the preparation of microgel samples, and all chemicals were purchased from Sigma-Aldrich, Norway AS and used as received. The chemicals, H_3PO_4, NaH_2PO_4, Na_2HPO_4, and Na_3PO_4, were used to prepare the buffer systems employed in this work, and they were all purchased from Sigma-Aldrich. Buffered solutions at pH values of 2, 7, and 11 were utilized in this study. All the buffers had a constant ionic strength of 0.05 M. The water employed in this investigation was purified with a Millipore Milli-Q system, and the resistivity was approximately 18 MΩ cm.

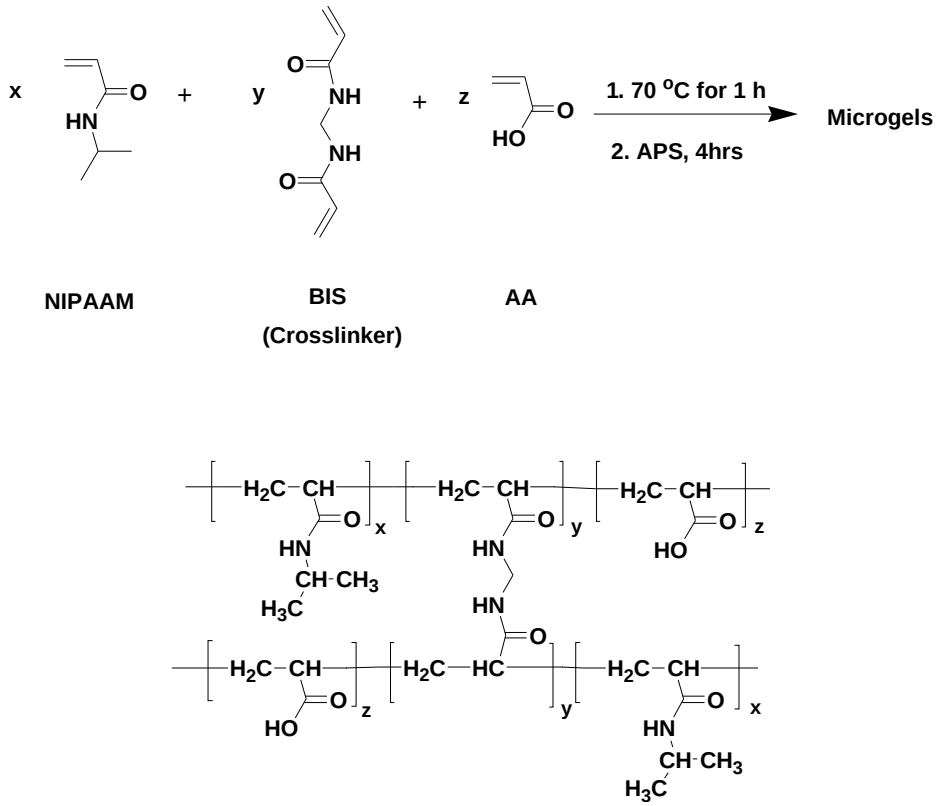

Figure 16: *Schematic illustration of the synthesis and chemical structure of the cross-linked PNIPAAM-co-PAA microgel system.*

For this purpose, we have synthesized uncharged PNIPAAM microgels cross-linked by *N*, *N*′-methylenebis(acrylamide) (BIS) and charged PNIPAAM microgels with different amounts of acrylic acid groups (PNIPAAM-*co*-PAA), see Figure 16. The characteristic data for the microgels are presented in Table 1.

Table 1. Characteristic Feed Ratio Data for the Synthesized Temperature- and pH-Responsive Microgels.

Sample Code	[NIPAAM] Mol-%	[BIS] Mol-%	[AA] Mol-%
MG-01	92	2	6
MG-02*	92	2	6
MG-03	98	2	0
MG-04	97	2	1

* The only sample that was synthesized in the presence of SDS (60 mg)

The results demonstrates that the interplay between intrapolymer and interpolymer aggregation can be tuned by changing factors such as the concentration of PNIPAAM, the incorporation of charged groups into the PNIPAAM microgels, or adding an ionic surfactant to a solution of PNIPAAM. In addition, effect of pH on the temperature-induced association behavior is analyzed [62]. We believe that the findings from this work provide us with a better understanding of the intricate competition between intrachain and interchain association in systems of thermally sensitive polymers.

III.1.2.1 Microgel Synthesis

A detailed route for preparation of microgels by free radical precipitation polymerization has been reported elsewhere [114]. A typical procedure can be briefly described in the following way. The total concentration of the monomers in the pregel sample

was kept constant at 70 mM, where 2 mol-% was BIS, 6 mol-% was acryl acid (AA), and the remaining 92 mol-% was NIPAAM. All monomers were dissolved in 600 mL of water and the resulting solution was filtered through a 0.1 μm membrane filter to remove particulate matter. The reaction mixture was first purged with nitrogen for 30 min to remove the dissolved nitrogen oxygen in a 1-liter 3-neck round bottom flask, equipped with a condenser and inlet for nitrogen. The mixture was then heated to 70 °C under a gentle stream of nitrogen for 1 h, after which 60 mg of APS dissolved in 5 mL of degassed water was added to initiate the reaction.

The reaction mixture became turbid about 1 min after the APS solution was added. The reaction mixture was kept at 70 °C for another 4 hours to complete the reaction. After cooling the reaction mixture down to room temperature, the microgel solution was filtered using fine porosity filter paper (Schleicher & Schuell GmbH) to remove possible aggregated material. The particles were then further purified by dialysis (Spectra/Por 6 dialysis membrane, MWCO 8,000) against water that was changed daily for at least 4 weeks to remove low-molecular weight impurities such as unreacted monomers, as well as minute rests of SDS (for MG-02) from the microgels. The microgel products were finally collected by lyophilization. It should be mentioned that in the preparation of MG-02, the polymerization reaction was conducted in the presence of SDS.

We note from Table 1 (page 41) that the microgel particles have the same degree of cross-linking and that the NIPAAM contents are almost the same. As frequently reported, the free radical precipitation polymerization produces nearly monodispers spherical particles in the sub-micron size range [114,115]. MG-03, was synthesized from a mixture of only NIPAAM and the cross-linker (BIS), and these microgels consist of only cross-linked NIPAAM chains without charges and MG-04, has a very low charge density. The two other microgels, MG-01and MG-02*, have both 6 mol-% of charged groups, but the MG-02* sample was prepared in the presence of SDS. As shown below, the microspheres from MG-

02* have a smaller size than all the other types of microspheres, because SDS stabilize the small precursor particles [116]. The polymerization reaction and the simple chemical structure of the PNIPAAM-*co*-PAA system are depicted in Figure 16 (page 40).

III.2 Mechanical Stirring

A beaker was filled with 100 mL 0.1 wt % HEC aqueous alkaline solution and the sample was exposed to a preset rotational speed in the range 0-400 rpm, and 15 μL/g of DVS was added to the solution to start the cross-linker reaction. For the sample with 0 rpm, a fast homogenization of the solution was performed (5 min at 50 rpm) before the stirrer was turned off. The cross-linker reaction in solutions of the polymer occurs between the cross-linker molecules and hydroxyl groups on the polymer chains.

At different times during the reaction at a prescribed rotational speed, 4 mL was withdrawn from the reaction mixture with a pipette, and this test sample was quenched rapidly by adding a few drops of concentrated HCl to the sample to lower the pH to acid conditions (pH ≈ 2) and thereby the cross-linker reaction was terminated. The same procedure to prepare the test solutions was repeated at all stirring speeds to ensure good reproducibility of the measurements.

III.3 Turbidity

For the HEC microgels, transmittances of quenched 0.1 wt % alkali solutions of HEC, exposed to different stirring speeds, at various stages during the cross-linker reaction at 25 °C were measured with the aid of a temperature-controlled Helios Gamma (Thermo Spectronic, Cambridge, UK) spectrophotometer at a wavelength of 500 nm. The apparatus is equipped with a temperature unit (Peltier unit) that gives a good temperature control over an extended time (25 ± 0.05 °C).

For the PNIPAAM-microgels, the influence of temperature on the transmittance of aqueous suspensions of the studied microgel systems was measured. In this work, the heating rate was set to 0.2 °C /min. The heating rate of the spectrophotometer was controlled by a PC that was interfaced to the apparatus and equipped with homemade software that gives the possibility of performing both temperature and wavelength scans with user-defined protocols.

The turbidity (τ) has been determined by Equation 1. The results from the spectrophotometer measurements will be presented in terms of turbidity.

III.4 Dynamic Light Scattering

The polymer solutions were filtered in an atmosphere of filtered air through 5 μm filters (Millipore) directly into pre-cleaned NMR tubes. For the NIPAAM-system, the DLS experiments were performed with a temperature gradient of 0.2 °C/min, as for the turbidity measurements. In this way the polymer was exposed to the same temperature conditions in both methods. The correlation function data were recorded continuously every 3rd min. When going back to 25 °C after the heating cycle, the values were the same as before the sample was heated. In addition, quenching measurements with DLS, where the temperature was changed very fast from a high to a low temperature revealed that the transition from one state to another is a fast process.

III.5 Rheo-Small Angle Light Scattering

Combined rheological and small angle light scattering Rheo-SALS experiments during shear flow were performed simultaneously using a Paar-Physica MCR 300 rheometer, equipped with a specially designed parallel plate-plate configuration (the diameter of the plate is 43 mm) in glass [117]. In all measurements a 10 mW diode laser operating at a wavelength of 658 nm was used as the light source, and a polarizer is placed in the front of the laser and an analyzer below the sample, making both polarized (polarizer and analyzer parallel) and depolarized (polarizer and analyzer perpendicular) experiments possible. All experiments in this study were conducted using polarized light scattering. Utilizing a prism, the laser beam was deflected and passed through the sample placed between the transparent parallel plates. The distance between the plates is small (0.5 mm) so that the effect of multiple scattering is less pronounced when the sample becomes turbid at long cross-linking times. The light is propagated along the velocity gradient direction, thus probing the structure in the plane of flow and vorticity. The forward scattered light at small angles was collected on a flat translucent screen below the sample (distance between sample and screen is 12.3 cm).

The 2D scattering patterns formed on the screen were captured using a CCD camera (driver LuCam V. 3.8), which plane is parallel to that of the screen. A Lumenera (VGA) CCD camera (Lumenera Corporation, Ottawa, Canada) with a Pentax lens was utilized, and the scattered images were stored on a computer using the StreamPix (NorPix, Montreal, Quebec, Canada) application software (version 3.18.5), which enables a real-time digitalization of the images. The images were acquired via the CCD camera with an exposure time of 200 ms. Subsequently, the pictures were analyzed using the SALS-software program (version 1.1) developed by the Laboratory of Applied Rheology and Polymer Processing, Department of Chemical Engineering, Katholieke Universiteit Leuven, Leuven, Belgium. The scattering

functions were recorded continuously during the run. The approximate accessible scattering wave vector (q) range is between $q = 4 \cdot 10^{-4}$ nm^{-1} and $q = 2 \cdot 10^{-3}$ nm^{-1}. The temperature of the instrument is controlled electronically to a high stability by using thermostated circulating water. All the Rheo-SALS measurements reported below are measured with an increasing shear rate.

III.6 Asymmetric Flow Field-Flow Fractionation

The asymmetric flow field-flow fractionation (AFFFF) experiments were carried out on an AF2000 FOCUS system (Postnova Analytics, Landsberg, Germany) equipped with an RI-detector (PN3140, Postnova) and a multiangle (7 detectors in the range 35^{o}-145^{o}) light scattering detector (PN3070, $\lambda = 635$ nm, Postnova). Measurements were performed on HEC samples (0.1 wt % samples, quenched from the reaction mixtures at various stages in the course of the cross-linking process) by using a 250 μm spacer, a regenerated cellulose membrane with a molecular weight cutoff of 10 000 (Z-MEM-AQU-427N, Postnova), and an injection volume of 20 μL. The measurements were conducted utilizing a constant detector flow rate of 0.2-0.8 mL/min and a slot-pump flow rate of 0.8-0.2 mL/min (the sum of the slot-pump flow rate and the detector flow rate was always 1.0 mL/min). The focusing time was 15 min at a cross-flow of 2 mL/min. Thereafter, the cross-flow was reduced linearly to 0.3 mL/min during a 3 min period. The cross-flow was then reduced exponentially (exponent of 0.3) to zero during a period of time of 7 min.

IV. RESULTS AND DISCUSSIONS

IV.1. HEC cross-linked by DVS

IV.1.1 Turbidity

Turbidity measurements have been carried out on dilute aqueous solutions of HEC in the presence of the cross-linker DVS. During the cross-linking process, the growth of large interpolymer aggregates will increase the turbidity of the solution. In this way the turbidity can be used as an indicator of the level of interchain cross-linking. Figure 17 shows that in the course of the cross-linker reaction of a 0.1 wt % HEC solutions in the presence of 15 μL/g of DVS, the samples become turbid. The results indicate that the formation of large aggregates is postponed to later times when the sample is exposed to higher stirring speed during the cross-linker reaction. The inset plot demonstrates that the cloud point time increases as the shear flow increases. This finding suggests that interchain association is delayed because shear forces make it more difficult for the chains to form interpolymer contacts. However, when most of the intramolecular cross-linking sites have been consumed, the frequent collision of the molecules will lead to the formation of large aggregates. Actually, at long reaction time the impact of rotational speed on the turbidity is modest.

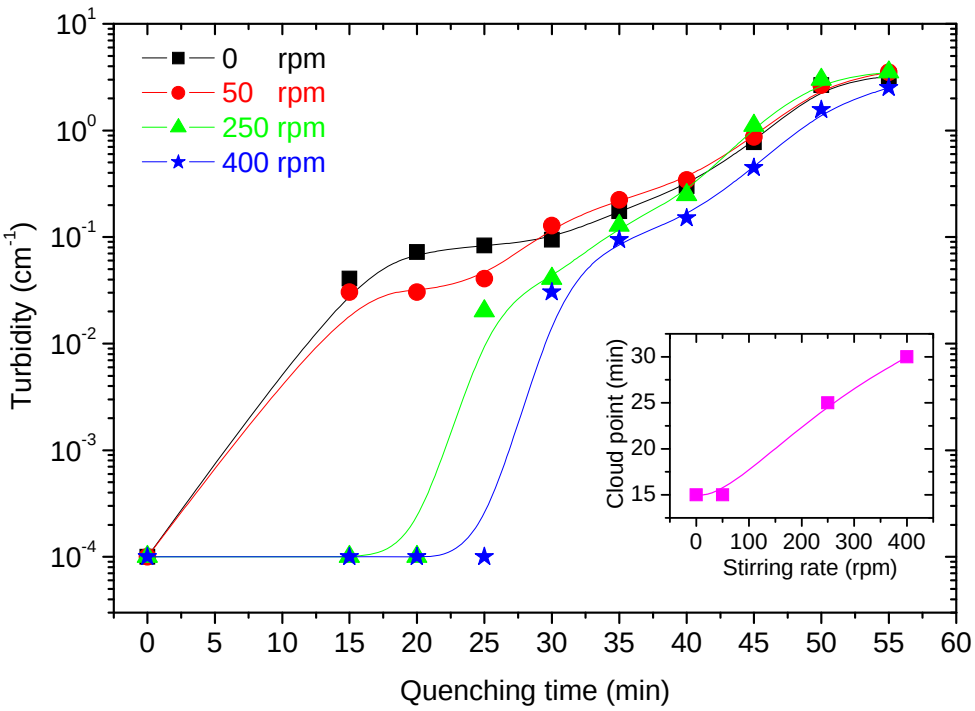

Figure 17: *Turbidity at different stages during the cross-linking of 0.1 wt % solutions of HEC in the presence of 15 μL/g DVS at the stirring speeds indicated. The inset plot shows the values of the cloud point determined from the incipient rise of the turbidity curve.*

IV.1.2 Dynamic Light Scattering

The time evolution of the normalized correlation function for 0.1 wt% HEC solutions in 0.05 M NaOH with and without cross-linker (15 μL/g DVS) at various stages during the cross-linking reaction at a stirring speed of 250 rpm depicted in Figure 18. The correlation functions are shifted toward longer times as the cross-linking process proceeds. The slower decay of the relaxation function at longer reaction times indicates the growth of large clusters. The same effect has also been observed for other systems of different natures [118-120]. In order to avoid multiple scattering effects [121] (multiple scattering is usually observed in turbid samples), DLS experiments are only carried out at relatively short reaction times. The inset plot in Figure 18 shows semi-logarithmic plots of $g^1(t)$ as a function of t^β for the quenching times indicated. This type of plot yields straight lines for functions that can be represented by a stretched exponential. We observe that, the long-time behaviors of the correlation functions are well described by straight lines.

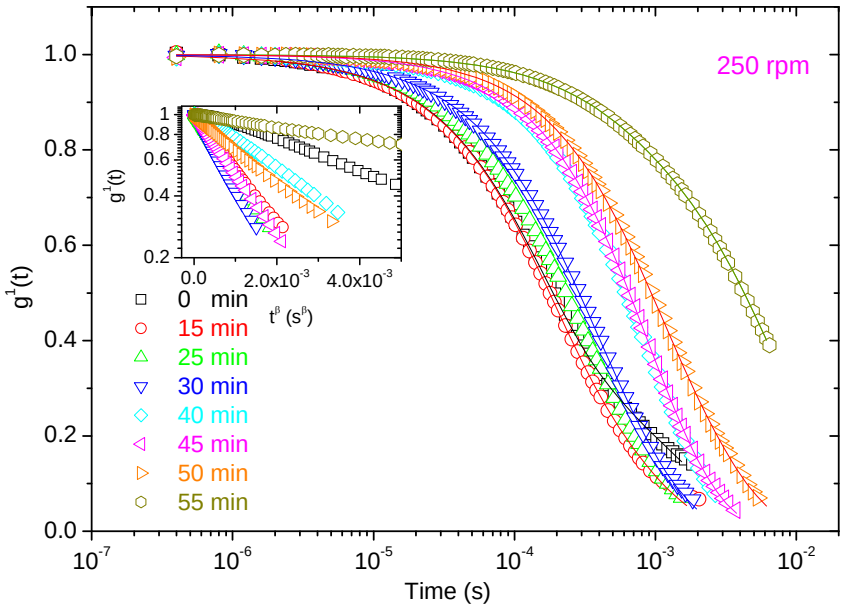

Figure 18: *Plot of the first-order electric field correlation function versus time at a scattering angle of 124 ^{o} for 0.1 wt % HEC in 0.05 M NaOH solutions with and without cross-linker (15 μL/g DVS) at various stages during the cross-linking reaction at the stirring speed indicated. . The solid lines are fitted by eq.5. The samples are quenched by adding a few drops of HCl to the solution to lower the pH to 2. The inset plot demonstrates the stretched exponential character of the correlation functions at long times.*

To scrutinize the goodness of the fitting procedure, and to endorse the functional form of the fitting algorithm eq. 5 that was employed to portray the correlation functions, residual plots from the fittings of a typical correlation function by using a single stretched exponential or eq. 5 are displayed in Figure 19. By fitting the correlation function by means of a single stretched exponential eq. 4, it is evident that the corresponding values of the residuals are large and the residual curve exhibits a systematic trend. This is a signature of a poor fit of the data. The random distribution and small values of the residuals by fitting the correlation function data with the aid of eq. 5 indicate good agreement between the fitting expression and

the data. This suggests a bimodal form of the correlation function as specified by eq. 5, where the fast mode portrays the diffusion behavior of the molecularly dispersed entities or small clusters, whereas the slow mode depicts motions of the large aggregates. Although, the population of the huge complexes dominates at the later stage of the cross-linker reaction, we are able at all instances to separate the contribution from the smaller species.

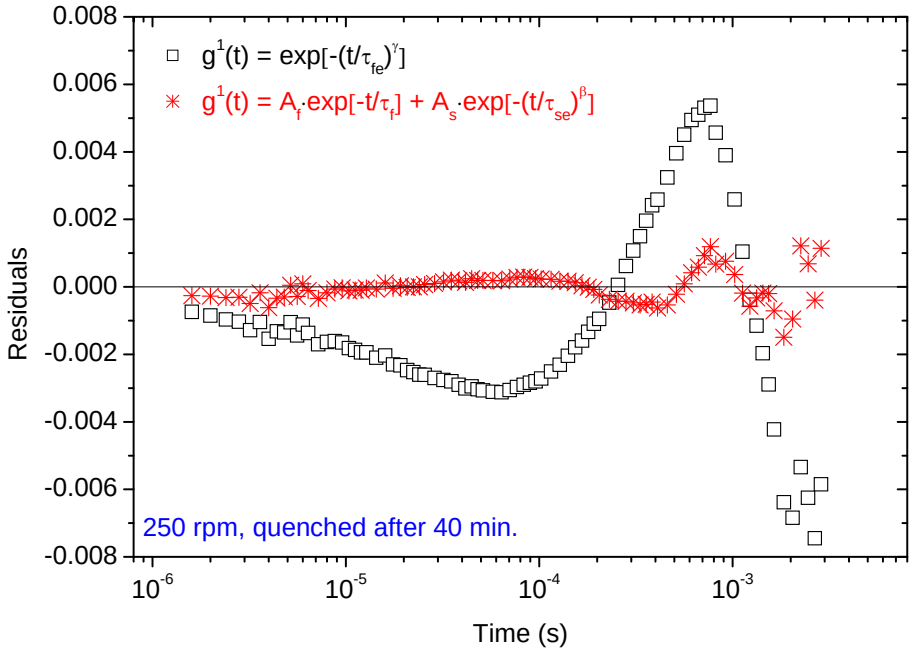

Figure 19: *Plot of the residuals by fitting a typical correlation function with the aid of one stretched exponential eq.4 or two eq.5.*

The q dependencies of the correlation functions are plotted against q^2t, see Figure 20. A diffusive mode is q^2 dependent. The correlation functions data for alkali 0.1 wt% HEC are collapsed onto a single curve, thus reflecting the diffusive character of both of the relaxation modes. If the relaxation modes are diffusive, the hydrodynamic radii ($R_{h,f}$, and $R_{h,s}$) can be calculated from the fast and slow relaxation times, respectively, via the Stokes-Einstein relationship eq. 7.

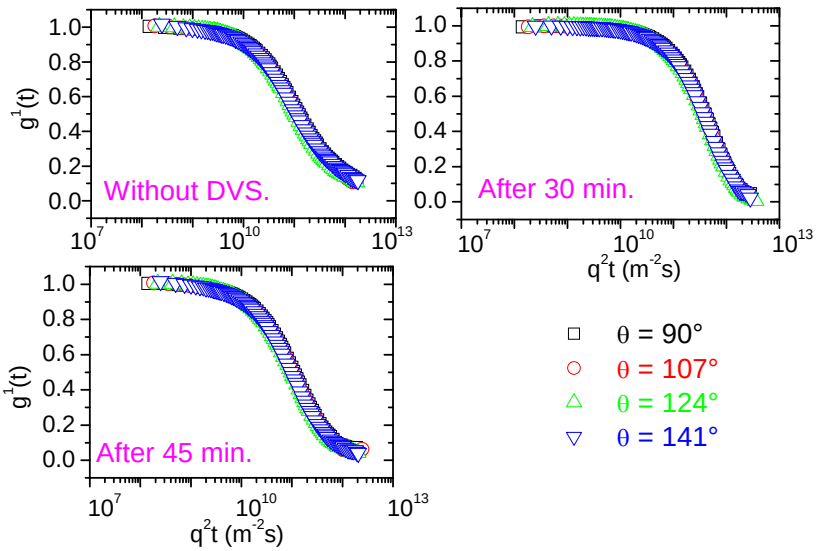

Figure 20: *Plot of the first-order electric field correlation function as a function of q^2t at the scattering angles indicated for 0.1 wt % HEC in 0.05 M NaOH with and without cross-linker (15 μL/g DVS) at various stages during the cross-linking reaction at the stirring speed 250 rpm.*

Normalized correlation function data for 0.1 wt % aqueous HEC solutions at various stages of the cross-linker reaction performed at two different stirring speeds, together with one solution without DVS (0 min), are depicted in the form of semilogarithmic plots in Figure 21. The general behavior is that the relaxation function is shifted toward longer times as the cross-linking process proceeds, and this trend is less pronounced with increasing stirring speed. The slower decay of the correlation function at long times reflects the growth of large clusters.

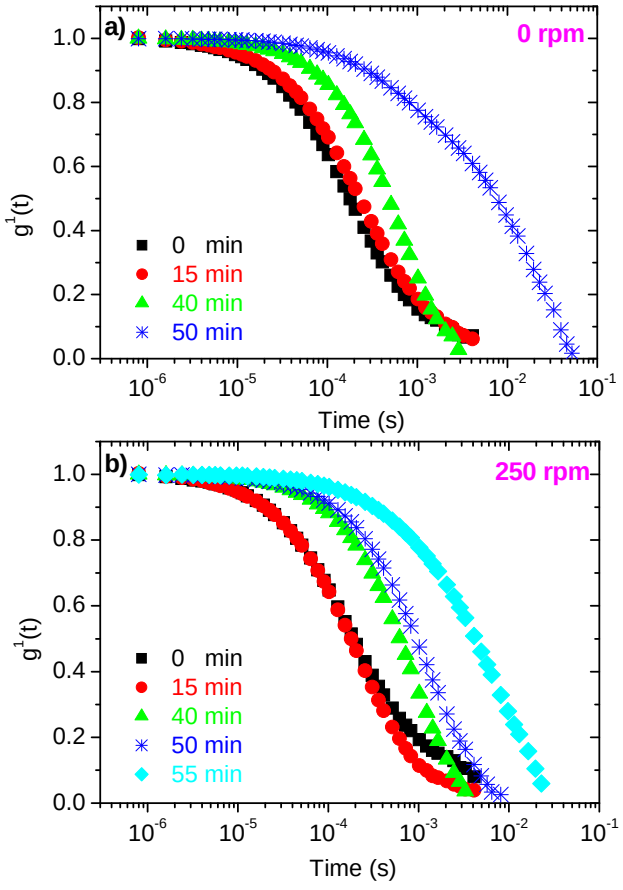

Figure 21: *Plot of the first-order electric field versus time (every second data point is shown) at a scattering angle of 124° for 0.1 wt % HEC solutions without and with cross-linker at various stages during the cross-linking reaction and for samples at two different rotational speeds (0 and 250 rpm).*

The hydrodynamic radii of the fast ($R_{h,f}$) and the slow ($R_{h,s}$) relaxation modes are depicted in Figure 22. It is obvious that at early times during the cross-linking process, the fast mode yields low values of $R_{h,f}$ but at later stages of the cross-linker reaction higher values of $R_{h,f}$ are observed. At later times in the course of the cross-linker reaction, the number of molecularly dispersed units will gradually become smaller and the population of minute clusters will affect the fast relaxation time. We note that the growth of these clusters is delayed to longer reaction times when the quenched solutions have been exposed to high stirring speeds.

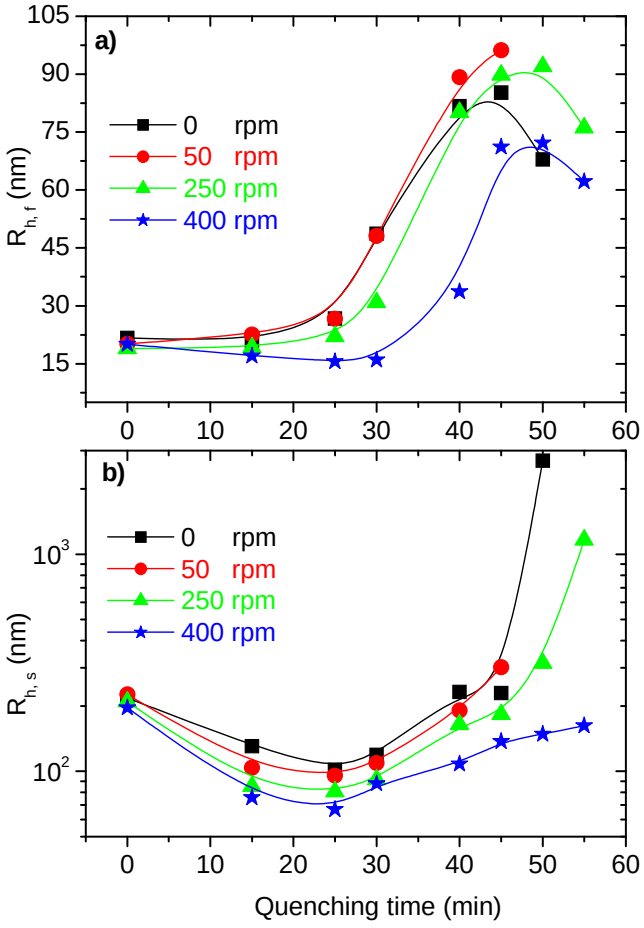

Figure 22: *Effect of stirring speed on the apparent hydrodynamic radii, determined from the fast mode ($R_{h,f}$) and the slow mode ($R_{h,s}$), for 0.1 wt % solutions of HEC at various stages during the cross-linking process.*

The apparent hydrodynamic radius, $R_{h,s}$, calculated from the slow relaxation time, represents the population of larger aggregates in the solution, see Figure 22b. It is interesting to note that at early times during the cross-linking process, the clusters contract and this phenomenon becomes significantly stronger for the sample that has been subjected to the highest stirring speed. This clearly shows that initially the larger complexes depicted by the slow relaxation mode are exposed to intrapolymer cross-linking, and this feature is strengthened under the influence of shear forces because this perturbation reduce the tendency to form interchain aggregates. This behavior is consistent with the shear viscosity results reported for this system previously [37]. At later times in the course of the cross-linker reaction, larger aggregates are formed, probably because most of the sites for intramolecular cross-linking have been consumed and the repeated collisions between the species have provoked interchain cross-linking. However, high shear stresses repress the tendency of forming massive aggregates even at long reaction times. These findings plainly reveal that a dilute polymer solution with a cross-linker agent is less disposed to build up interpolymer cross-links under the influence of vigorous stirring.

In connection with EOR applications it is important that the particles are stable over an extended temperature domain. By plotting the correlation function data against the quantity tT/η_0 (where T is the absolute temperature and η_0 is the solvent viscosity), trivial changes of the solvent viscosity with the temperature have been taken into account. Since the correlation data at all temperatures virtually condense onto each other, the effect of temperature on the diffusion behavior of the particles can be neglected see Figure 23a. The long-term stability was checked at a temperature of 25°C, over a time period of five months. As can be seen from Figure 23b, the sizes of the microgels are relatively stable over a long time period.

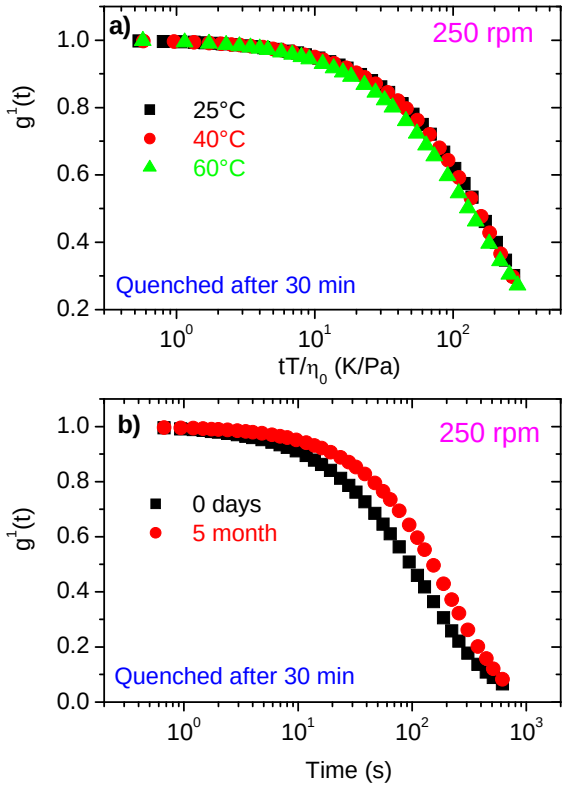

Figure 23: *a) Plot of the first-order electric field correlation function as a function of tT/η_0 for cross-linked particles of 0.1 wt % HEC in 0.05 M NaOH cross-linked by 15 μL/g DVS. The stirring speed was 250 rpm, and measured at a scattering angle of 90° at the temperatures indicated b)Plot of $g^1(t)$ versus time measured at the same day as the sample was cross-linked, and after 5 months at 25 °C.*

IV.1.3 Rheo-Small Angle Light Scattering

This type of technique can provide us information about structural changes of cross-linked complexes on a global dimensional scale under the influence of shear flow. By this experimental method, it is possible to monitor shear-induced aggregation or disintegration of species in situ. Figure 24 illustrates the 2D-scattering patterns at different shear rates and cross-linking stages for 0.1 wt % HEC solutions that have been exposed to various stirring speeds during the cross-linking process. For the solution in the quiescent state that has been quenched after 50 min, the species are broken up under the influence of shear, whereas clusters that are more stable against shear forces are evolved when the reaction mixture was subjected to a high stirring speed. At this stage of the cross-linker reaction, the high collision frequency of the polymer entities seems to buildup multichain aggregates that are more stable against mechanical stresses. After a sufficiently long reaction period, the scattered intensity is strong and huge aggregates are formed, both for the solution in the quiescent state and for the solution exposed to a high stirring rate. These association complexes are practically not affected by neither the stirring speed nor by the subsequent shear forces. In the considered wave vector range, most of the SALS patterns are virtually isotropic, which suggests that on this dimensional scale no major structural alterations occur.

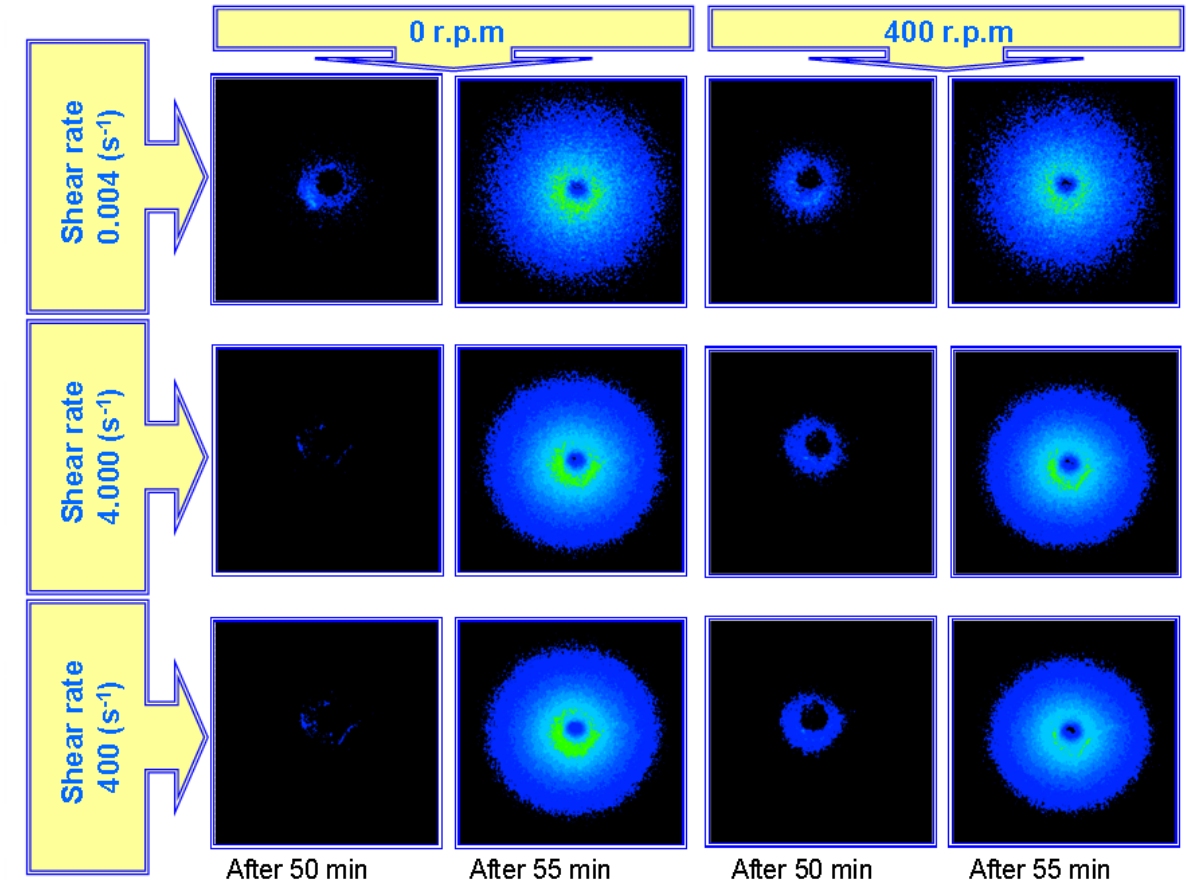

Figure 24: *2D SALS patterns at various shear rates of 0.1 wt % HEC solutions at different stages of the cross-linker reaction of mixtures exposed to two different stirring speeds.*

To elucidate the impact of shear flow on the formation of structures at various stages in the course of the cross-linking process, shear rate dependences of the scattered intensity (at a fixed q value of 0.27 μm^{-1}) for 0.1 wt % solutions of HEC in the presence 15 μL/g DVS that have been exposed to a constant stirring speed of 250 rpm are depicted in Figure 25a. For the HEC solution (0.05 M NaOH) without DVS, the scattered intensity is practically unaffected by the shear flow, which indicates that no significant structural changes of the molecules occur. The moderate upturn of the scattered intensity at high shear rates are ascribed to incipient turbulence. For solutions at early states of the cross-linker reaction, the scattered intensity drops at higher shear rates. As the cross-linking process advances, the intensity at low shear rates increases and the intensity falls off at higher shear rates. This scenario suggests that aggregates are broken up at higher shear stresses, whereas stronger association complexes are formed as the cross-linker reaction proceeds. Actually, when massive aggregates have been formed the intensity is virtually unaltered with increasing shear flow over the considered shear rate interval. This finding supports the conjecture that more sturdy complexes are formed at later state during the cross-linking process.

A comparison of the effect of stirring speed on the scattered intensity during the cross-linker reaction for 0.1 wt % HEC solutions at two different times of quenching is depicted in Figure 25 b,c. At the earlier state of quenching, the species from the reaction mixture that has been subjected to a lower stirring speed are disintegrated at a high shear rate, whereas virtually no alteration of the scattered intensity with increasing shear rate occurs for the sample exposed to a higher stirring speed. This finding supports the idea that the more intense collision of species at a higher stirring speed leads to more compact objects that are less disposed to breakup under the influence of shear stresses. At a later state of the cross-linking process (Figure 25c), the scattered intensity is independent of shear rate at both stirring speeds. This observation indicates that as the cross-linking reaction proceeds, more stable aggregates are formed that can withstand the applied shear forces.

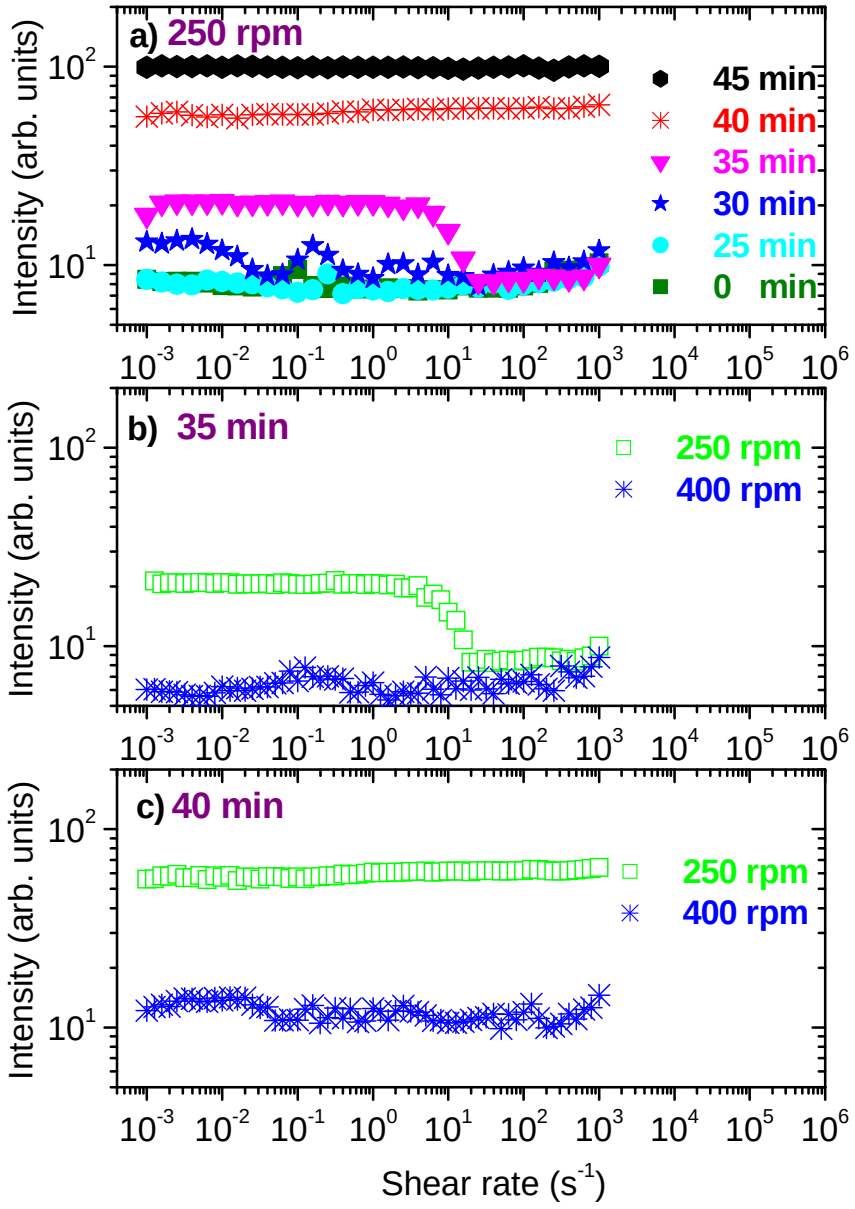

Figure 25: *a) Shear rate dependences of the scattered intensity (at a fixed q value of 0.27 μm^{-1}) at different stages during the cross-linker reaction (15 μL/g DVS) for 0.1 wt % solutions of HEC that have been subjected to a stirring speed of 250 rpm in the course of the cross-linking process. b), c) Effects of shear rate and stirring speed on the scattered intensity at two different stages in the course of the cross-linking process.*

IV.1.4 Asymmetric Flow Field-Flow Fractionation

Figure 26 shows the effects of the reaction time and stirring rate on the weight-average molecular weight and the polydispersity index (M_w/M_n) for 0.1 wt % HEC solutions. This information is usually difficult to obtain, but with the aid of AFFFF it is possible to gain insight into these features. It is evident from Figure 26a that the molecular weight increases in the course of the cross-linker reaction. This feature suggests that giant interpolymer complexes are formed as the reaction proceeds, but as discussed above the growth of these clusters is repressed under the influence of a high stirring speed. This finding is compatible with the results from DLS. The coexistence between the formation of intrachain and interchain cross-links during the cross-linker reaction is expected to yield species of various sizes. This is supported by the results in Figure 26b, but higher stirring speeds seem to produce species with much less polydispersity. This can probably be ascribed to disintegration of very large aggregates at high shear flows, and this yields a more narrow distribution of sizes. These results indicate that a high stirring speed yields both smaller aggregates and less polydispersity.

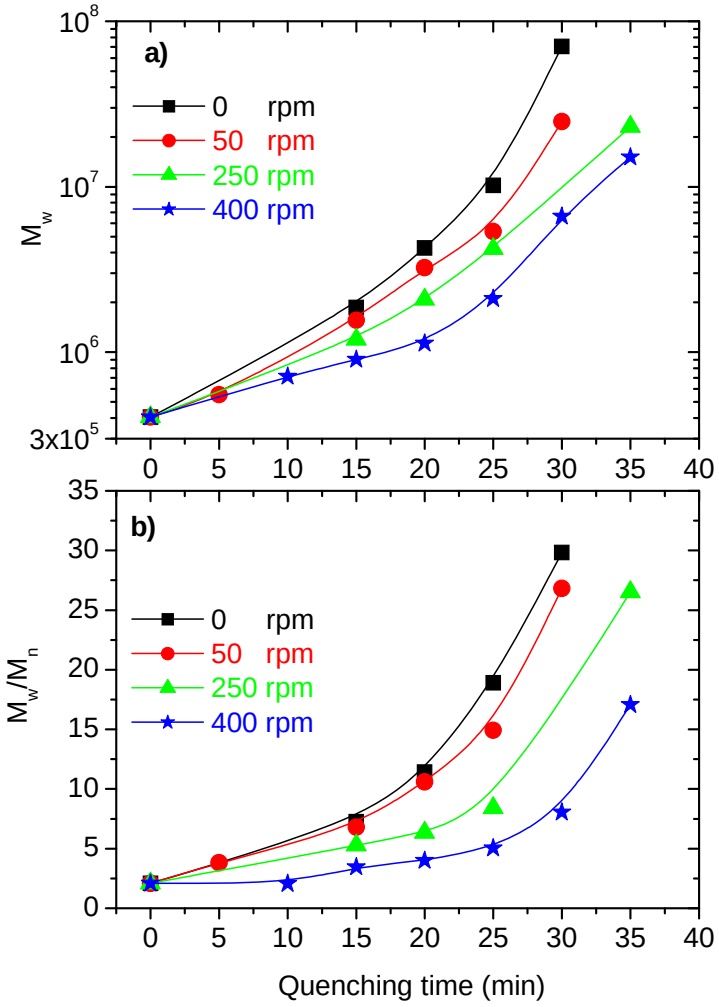

Figure 26: *Time evolution of the molecular weight and the polydispersity index determined from AFFFF for 0.1 wt % HEC solutions at various stages during the cross-linker reaction and under the influence of different stirring rates.*

IV.2 PNIPAAM cross-linked by BIS

The stability of microgels is a vital issue in many applications, and below we will elucidate the delicate temperature-induced shrinking and aggregation of microgels at various conditions. Effects of polymer concentration, addition of an ionic surfactant, incorporation of charged acrylic acid groups, and pH on the intra- and interpolymer association of microgel particles are discussed below.

The time evolution of the normalized correlation function for 0.04 wt% suspensions of uncharged PNIPAAM and charged PNIPAAM-co-PAA microgels, with different mol-% of acrylic acid (AA) groups are depicted in Figure 27. The sample synthesized in the presence of SDS (6 mol %, AA*) has a faster relaxation than the other systems, indicating that this synthesis procedure result in microgels with a smaller size. The inset plot shows that this system is well described by eq.4, see section IV.1.2 for more details.

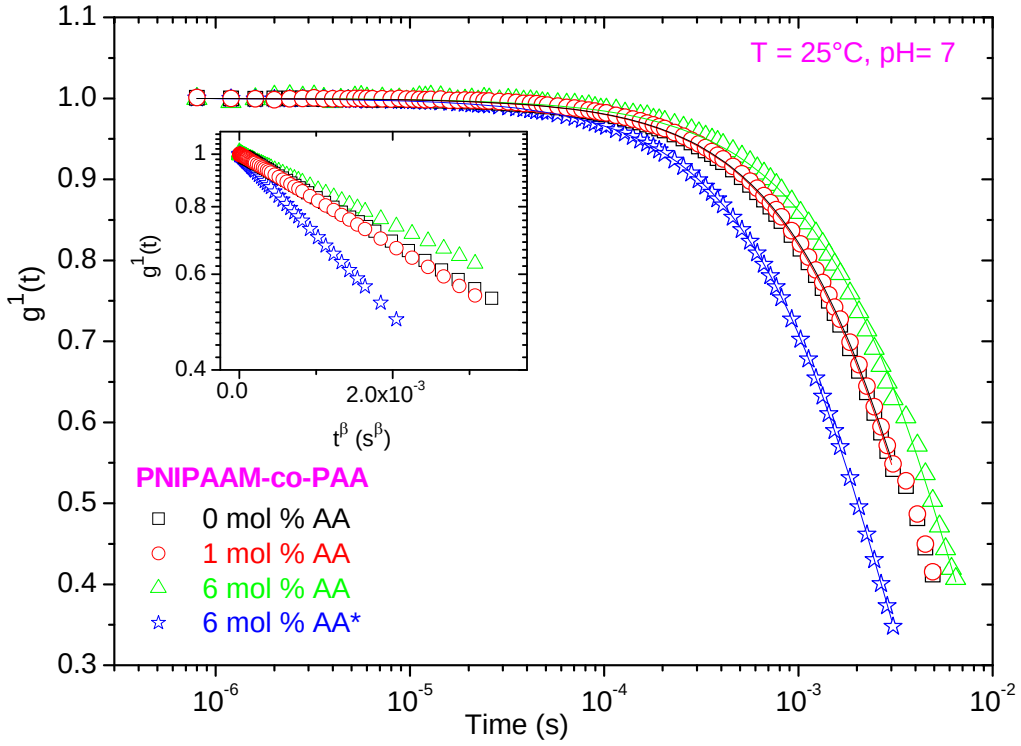

Figure 27: *Plot of the first-order electric field correlation function versus time at a scattering angle of 90° for 0.04 wt% suspensions of the uncharged PNIPAAM and the charged PNIPAAM-co-PAA microgels, with different mol-% of acrylic acid (AA) groups, at 25 °C and pH=7 in a buffer system of constant ionic strength (0.05 M). The solid lines are fitted by eq.4. The inset plot demonstrates the stretched exponential character of the correlation functions at long time.*

The angular dependence of the normalized correlation functions, for a 0.04 wt % suspension of the charged PNIPAAM-co-PAA microgels with 6 mol% of acrylic acid (AA), which was synthesized in the presence of SDS is illustrated in the form of a reduced plot in Figure 28. The same type of behavior is also observed for the other microgel systems. This indicates that the systems are q^2-dependent, i.e., diffusive, as explained in section IV.1.2.

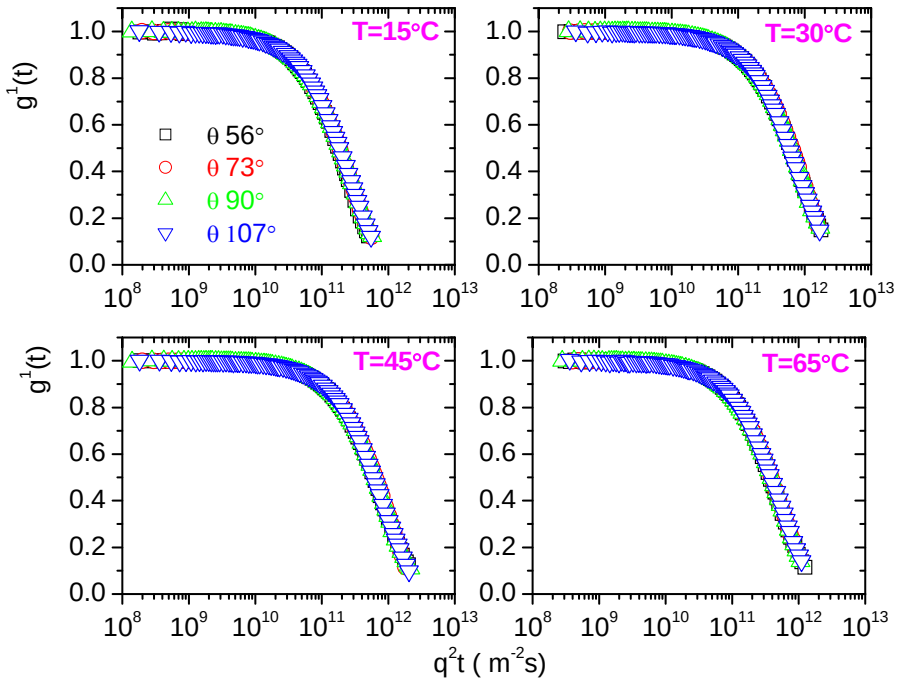

Figure 28: *Plot of the first-order electric field correlation function as a function of q^2t at the scattering angles indicated for a 0.04 wt % suspension of the charged PNIPAAM-co-PAA with 6 mol% of acrylic acid (AA) groups, which was synthesized in the presence of SDS. The measurements were carried out at pH = 7, at the temperatures indicated.*

IV.2.1 Effect of pH

To study the influence of charge density and pH on the association behavior of the temperature sensitive microgels, DLS and turbidity measurements have been conducted on 0.04 wt % suspensions of PNIPAAM and charged PNIPAAM-*co*-PAA microgels, with different mol-% of the acrylic acid groups (AA), in buffer systems of fixed ionic strength (0.05 M) at pH values covering both the acid and basic domain.

IV.2.1.1 Turbidity

The temperature dependency of the turbidity at different pH values for the various microgels is depicted in Figure 29. A general trend for the samples with low charge density (0 mol-% AA and 1 mol-% AA) at all pH values is the sharp transition in the turbidity at temperatures near LCST of PNIPAAM. These suggest the formation of giant clusters of particles. At pH = 2, this transition is also observed for the particles with 6 mol % AA, because the charges are neutralized at this pH. At pH = 7 and pH = 11, the turbidity of the systems with 6 mol-% AA groups, show moderate upturns at high temperatures. This suggests that the tendency of forming large aggregates is reduced due to charge stabilization of the microgels.

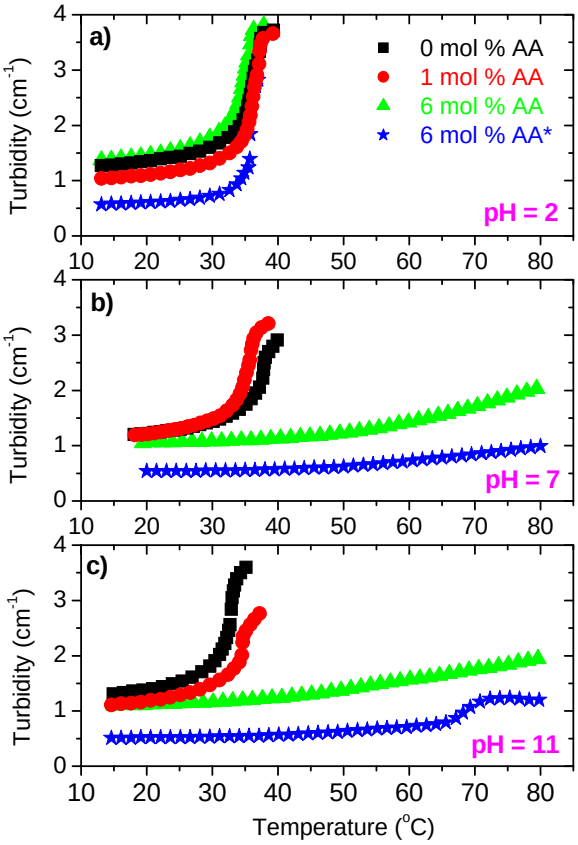

Figure 29: *Temperature dependences of the turbidity for 0.04 wt % suspensions of the uncharged PNIPAAM and the charged PNIPAAM-co-PAA microgels, at different mol-% of the acrylic acid (AA) groups, at the pH values indicated in buffer systems (0.05 M). The asterisk (6-mol% AA*) denotes that the sample that has been synthesized in the presence of SDS.*

IV.2.1.2 Dynamic Light Scattering

The results from DLS are collected in Figure 30. The influence of charge density on the size of the microgels at neutral (pH = 7) conditions is displayed in Figure 30b. A low charge density (1 mol-% AA) has practically no effect on the temperature dependency of R_h. Compared to the microgels with 0 or 1 mol % charge, the PNIPAAM microgels with 6 mol-% AA groups, swell at low temperatures due to electrostatic repulsion between the negatively charged carboxylate residues (pK_a of AA is ca.4) [122], whereas at a monotonous compression of the species takes place as the temperature increases as consequence of

enhanced hydrophobic interactions. The charges on the surfaces of the microgels suppress the tendency of forming aggregates. For the PNIPAAM-*co*-PAA sample (6 mol-% AA) that has been synthesized in the presence of SDS, the values of R_h are significantly lower than for the other samples and the microgels are compressed as the temperature increases, this results are compatible with what was observed for the turbidity. It is well known [123,124] that a surfactant as SDS acts as an efficient stabilizer of the particles during the cross-linker reaction and thus prevents the particles from coagulating. Therefore the microgels synthesized in the presence of SDS are significantly smaller than those synthesized without SDS.

At acid conditions (pH = 2) and low temperatures, R_h exhibits a pronounced drop at moderate temperatures which is similar as that for the sample at neutral pH, but in this case all systems show macroscopic phase separation slightly above the LCST of PNIPAAM (~ 32 ^oC), see Figure 30a. This is due to the neutralization of the AA-groups at low pH-values combined with the enhanced hydrophobicity of PNIPAAM at elevated temperatures.

At strongly basic conditions (pH = 11), the main features of R_h are similar as those at neutral pH, see Figure 30c. At higher pH values, the microgels are expected to swell because of the ionization of the carboxylic acid groups. A close inspection of the data, actually reveals that the values of R_h at low temperatures for the PNIPAAM with 6 mol-% AA groups are higher than the corresponding ones at pH = 7. At temperatures above LCST of PNIPAAM, the corresponding values of R_h are lower at pH = 11, because of more effective stabilization of the particles at a higher degree of ionization.

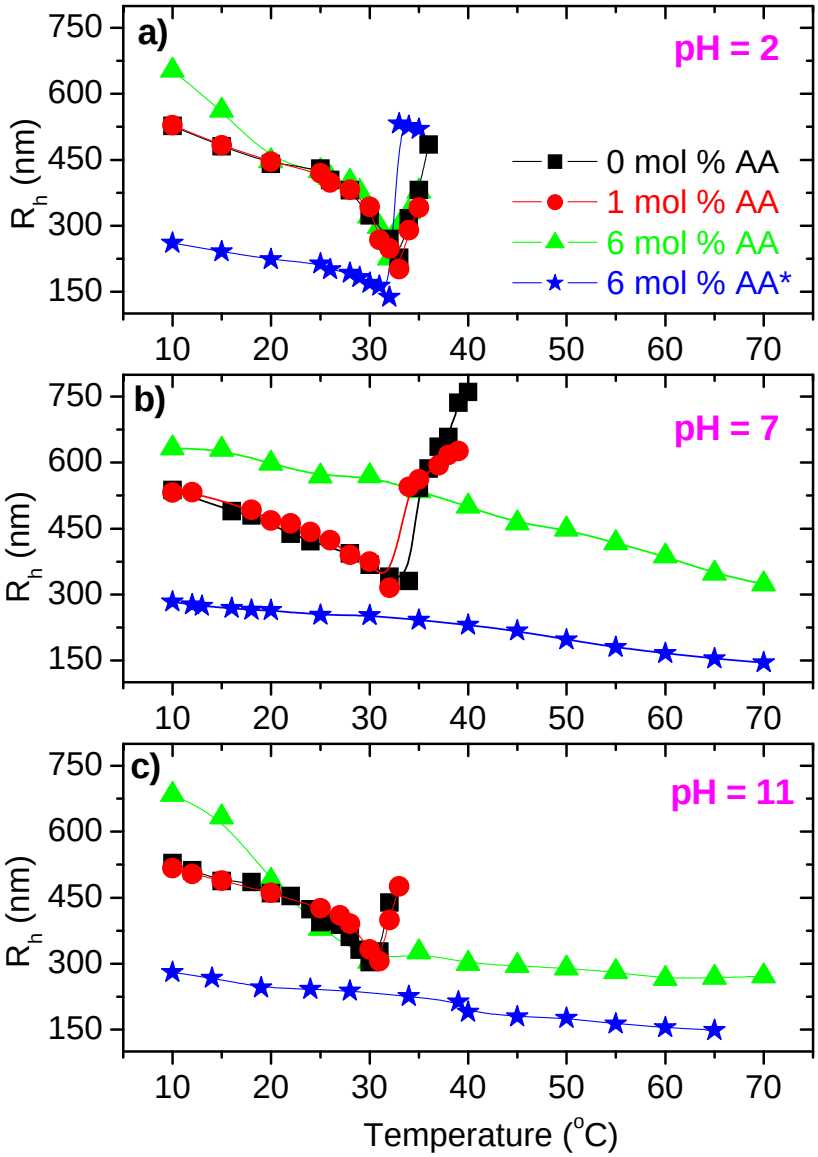

Figure 30*: Plot of the hydrodynamic radius as a function of temperature for 0.04 wt % suspensions of the uncharged PNIPAAM and the charged PNIPAAM-co-PAA microgels, at different mol-% of the acrylic acid (AA) groups, at the pH values indicated in buffer systems (0.05 M). The asterisk (6-mol% AA*) denotes that the sample has been synthesized in the presence of SDS.*

IV.2.2 Effect of Concentration

IV.2.2.1 Turbidity

The effect of temperature on the turbidity for suspensions of PNIPAAM microgels of various concentrations is depicted in Figure 31. The general picture that appears is that the turbidity values at low temperatures increase with polymer concentration, and the transition zones, with enhanced values of τ, for the different polymer concentrations are located at approximately the same temperatures independent of concentration. For the two highest concentrations, the upturn of τ is very strong at high temperatures, suggesting a development of huge clusters and a subsequent phase separation. At the lower concentrations, the turbidity curves level out at elevated temperatures. This trend indicates that the growth and collapse of the species cancel each other out. The inset plot shows that at a very low concentration, the turbidity is almost independent of temperature in the range 15-37 °C. The turbidity increases as the concentration is raised, and at temperatures above the LCST of PNIPAAM, this effect is much more pronounced.

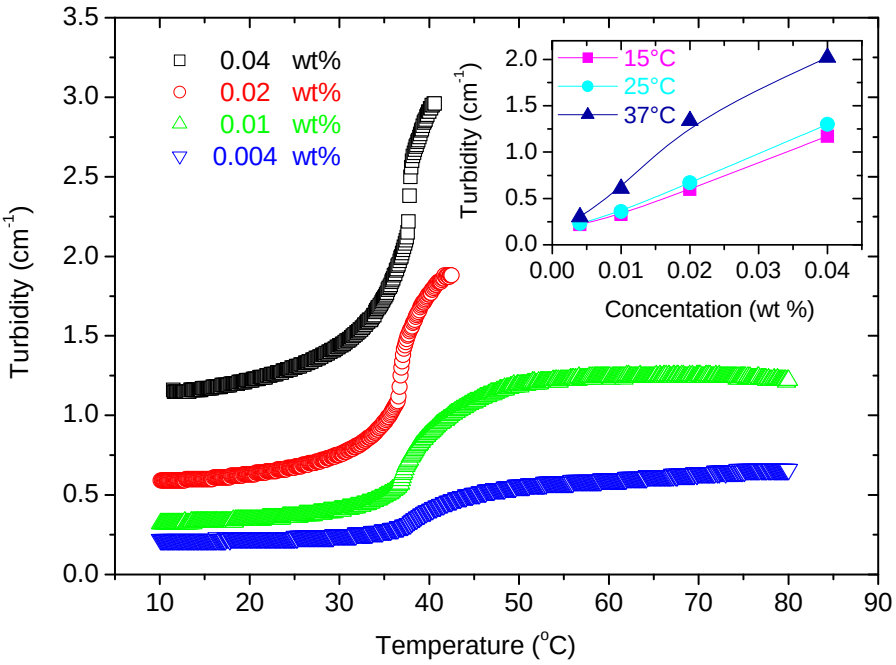

Figure 31: *Temperature dependency of the turbidity for different concentrations of aqueous suspensions of uncharged PNIPAAM microgels at pH = 7. The inset plot shows the turbidity as a function of the microgel concentration at the temperatures indicted.*

In the analysis of the turbidity results, we may resort to theoretical approaches [125,126] elaborated for spherical colloidal particles. The following expression was derived [126] for the turbidity $\tau = 3cQ_{ext}/(2d\rho)$, where c is the mass concentration (g/cm^3), Q_{ext} is the Mie extinction efficiency, d is the particle diameter, and ρ is the density of the particles. It is reasonable to assume at temperatures below the LCST that the mass m of the spherical particles of volume V is constant. In view of this, we can write $\rho = m/V$, where $V = (4/3)\,\pi\,(d/2)^3$. By inserting this in the expression above, we arrive at: $\tau = c\,Q_{ext}\pi d^2/4m$. This relation readily explains the raise of τ with increasing polymer concentration, and the strong increase of τ upon augmented aggregation at higher concentrations and temperatures. However, the significant temperature-induced collapse of the microgels observed from the DLS

experiments at temperatures below the LCST (the average size of the microgels decreases from approximately 500 nm to 300 nm in the temperature interval from 10 ^{o}C to 33 ^{o}C) is not directly reflected in the turbidity data Figure 31. To interpret this result in the framework of the equation above, it is necessary to argue that the value of Q_{ext} should increase with increasing temperature because the parameters c and m for a given concentration should be constant. The parameter Q_{ext} cannot easily be determined experimentally, but its value is a function of the relative refractive index n_p/n_0 (n_p is the refractive index of the spherical particle and n_0 is the refractive index of the solvent), and the value of Q_{ext} increases with increasing value of the quantity n_p/n_0. It is not unreasonable to presume that the refractive index of the particles increase during the compression stage, and this can therefore lead to an increase of τ in the initial stage (from 10 ^{o}C to 33 ^{o}C). To elucidate the impact of a change of the relative refractive index, it may be instructive to consider a relevant example and use the data presented in Figure 32a. If we use the same wavelength (λ = 500 nm) as in the present turbidity measurements, the ratio $\pi d/\lambda$ (on the x-axis in Figure 32) is altered from 3.1 to 1.9 as the particle size is changed from 500 nm to 300 nm. If we assume that the corresponding value of n_p/n_0 is changed from 1.05 to 1.10, the value of τ is increased by almost a factor of 2, in spite of that the size of the microgel drops from 500 nm to 300 nm. For the highest polymer concentration (0.04 wt %) considered here, the increase observed for the value of τ is ca. 30 % in the interval from 10^{o}C to 33^{o}C. This indicates that the variation of the value of n_p/n_0 upon the temperature-induced compression is less than in the invented example above.

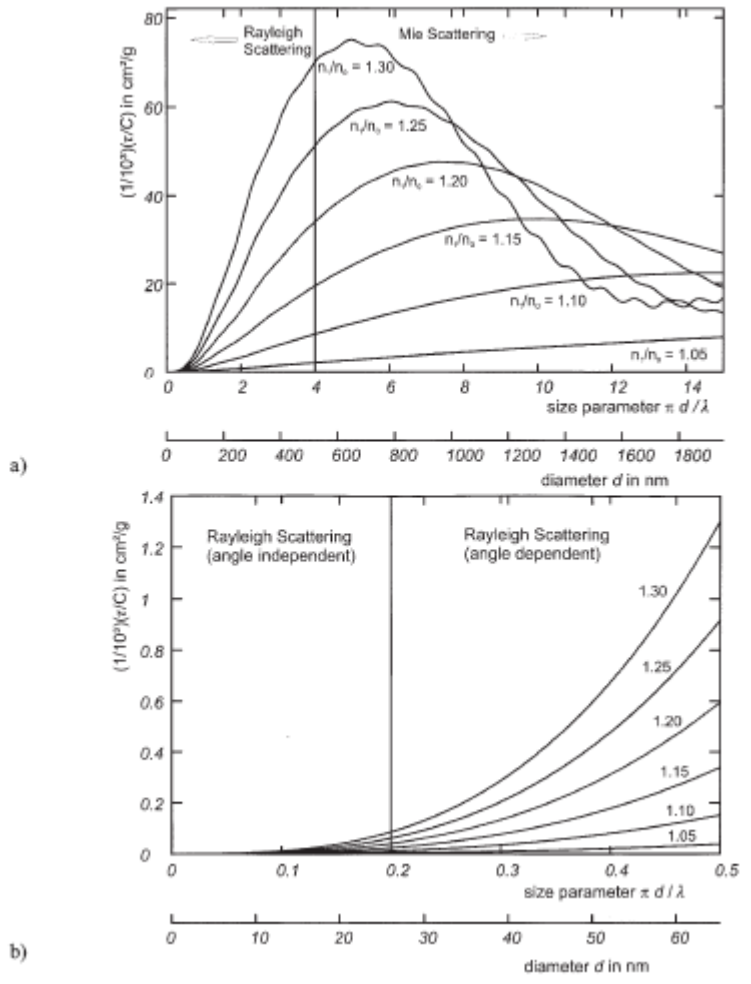

Figure 32: *Specific turbidity ε = τ/c for spheres as a function of the size parameter π d/λ for different relations of the refractive indices n_1/n_0: a) for 0 < π d/λ < 15. b) For 0 < π d/λ < 0.5.Tthe lower diameter axis d refers to λ_0 = 546.1 nm and n_0 = 1.333.* ***This Figure is taken from ref. 126 Figure 2.***

IV.2.2.2 Dynamic Light Scattering

In Figure 33a, normalized time correlation function data at a scattering angle of 90^o for aqueous suspensions of PNIPAAM microgels of various concentrations at a temperature of 40^oC, together with the corresponding curves fitted with the aid of eq. 4, are depicted in the form of semilogarithmic plots. Although enhanced aggregation occurs at this temperature for the higher polymer concentrations, the decays can almost be described by a single exponential ($\beta \geq 0.94$). This indicates a narrow distribution of sizes even when large clusters are formed. A comparison of the correlation functions clearly unveils a progressive slowing down of the relaxation process as the concentration increases. This tendency reflects the formation of large interchain association structures at this temperature and high concentration.

The general feature of R_h for all polymer concentrations is the marked collapse of the microgels at moderate temperatures, see Figure 33b. At low temperatures, the curves virtually condense onto each other, except for the highest polymer concentration where the augmented values of R_h indicate that some smaller aggregates have been formed even at low temperatures. The temperature-induced shrinking of the gel-particles can be accounted for in the following way. The isopropyl side group carried by each monomer of PNIPAAM confers a degree of hydrophobic character, whereas the hydrophilic nature of the polymer is established through hydrogen bonding of water with the amide groups. At elevated temperatures, the hydrogen bonding with water is gradually disrupted on heating and the hydrophobicity of the polymer is enhanced with packing of the hydrophobic segments, leading to progressive chain collapse [123,127]. This contraction behavior of the microgels is redolent of the coil-to-globule transition reported [128-130] for single chains of high molecular weight of PNIPAAM in very dilute solution.

At temperatures above the LCST of PNIPAAM (~ 32^oC), the temperature dependence of R_h is strongly affected by the polymer concentration, with an abrupt rise of R_h for the

highest concentration and almost no effect of temperature on R_h for the lowest concentration. This finding can be rationalized in the following scenario. At elevated temperatures, a situation of a perpetual competition between contraction of the microgels and interchain association evolves. At temperatures above the LCST, the hydrophobic stickiness of the species is enhanced and the higher sticking probability at high concentration promotes the formation of large aggregates. For the higher two concentrations, aggregation is the predominant phenomenon at elevated temperatures and macroscopic phase separation is approached. However, for an intermediate polymer concentration of 0.01 wt % the delicate interplay between building up interpolymer complexes and intrachain shrinking is reflected by the peak centered on 40 ^{o}C Figure 33b. For the lowest concentration, the collision frequency of spheres is low and the tendency of forming aggregates is repressed. These results clearly show that intrachain contraction and interchain association coexist at elevated temperatures, and these features are strongly governed by the polymer concentration.

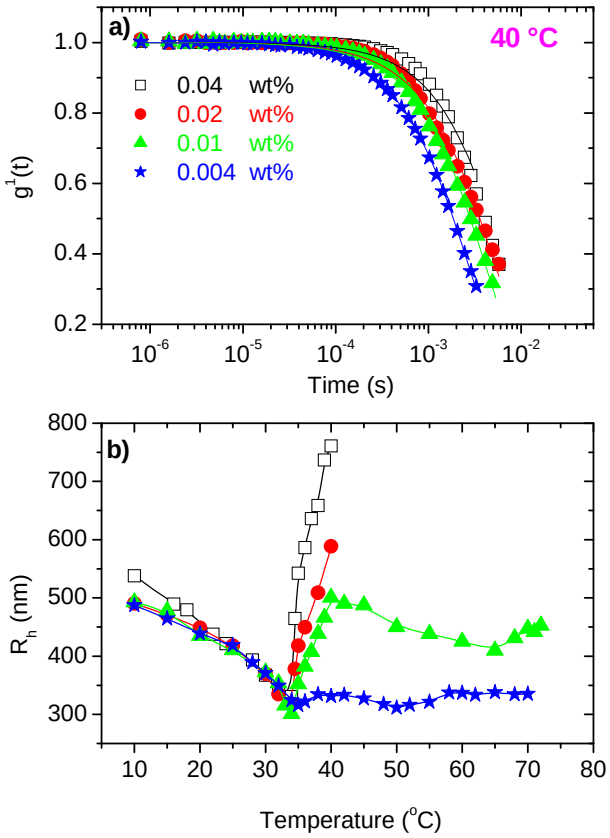

Figure 33: *a) First-order electric field correlation versus time (every second data point is shown) at a scattering angle of 90 ^{o} for aqueous suspensions of uncharged PNIPAAM microgels of different concentrations at pH = 7 and at a temperature of 40 ^{o}C. The solid lines are fitted by eq.4. b) The temperature dependences of the hydrodynamic radius.*

IV.2.3 Effect of Surfactant

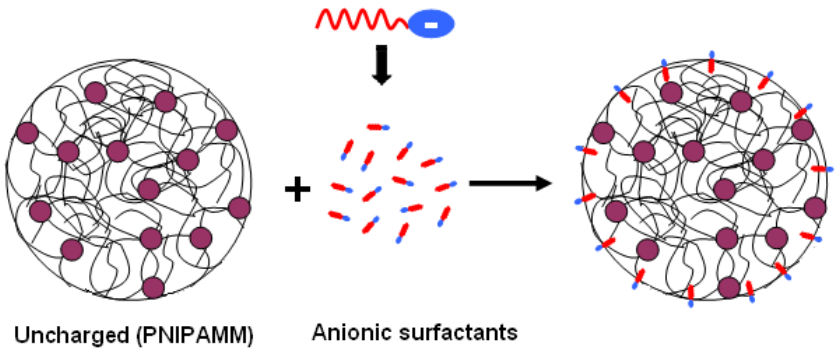

Figure 34: *An illustration of microgel-surfactant interactions.*

When an ionic surfactant, such as SDS, is added to uncharged PNIPAAM microgels, it has been argued [131] that the isopropyl side groups carried by each monomer of PNIPAAM is responsible for the interaction and binding of SDS to the polymer, see Figure 34. The adsorption of the surfactant onto the surface of the microgel gives rise to a polyelectrolyte behavior.

IV.2.3.1 Turbidity

The effect of temperature on the turbidity for a 0.04 wt % suspension of PNIPAAM, with and without SDS, is depicted in Figure 35a. In the absence of surfactant, a macroscopic phase separation occurs at temperatures above 40^{o}C. At a low surfactant concentration (~ 0.25 m*m*) both the macroscopic phase separation and the cloud point are found at a lower temperature than for the microgel without SDS. This trend is probably due to hydrophobic interactions between surfactant molecules and the hydrophobic groups in the microgel causing enhanced hydrophobic associations. When the SDS concentration is further increased, both the CP and the macroscopic phase separation temperature are shifted toward higher temperatures. This effect can be ascribed to the binding of surfactant to the polymer, thereby imposing repulsive interactions between the microgels particles. In this process a polymer-

ionic surfactant complex with a polyelectrolyte character is formed, and the aggregation is suppressed, causing higher cloud point temperatures, see Figure 35b. The minimum observed for the CP on the addition of SDS has also been observed for EHEC in the presence of this surfactant [70,132]

The effect of SDS concentration on the turbidity at different temperatures is depicted in Figure 35c. At a low temperature (15 °C), the turbidity increases with increasing the SDS concentration. The higher values of τ for PNIPAAM in the presence of surfactant can probably be ascribed to a slight expansion due to solubilization of the hydrophobic moieties for particles that are cross-linked inside with SDS. As the temperature is increased, a pronounced turbidity maximum at low SDS concentration is developed. This maximum can be related to the minimum in the CP (Figure 35b). When the SDS concentration is low, the CP decreases causing the turbidity at elevated temperatures to increase as a function of SDS concentration.

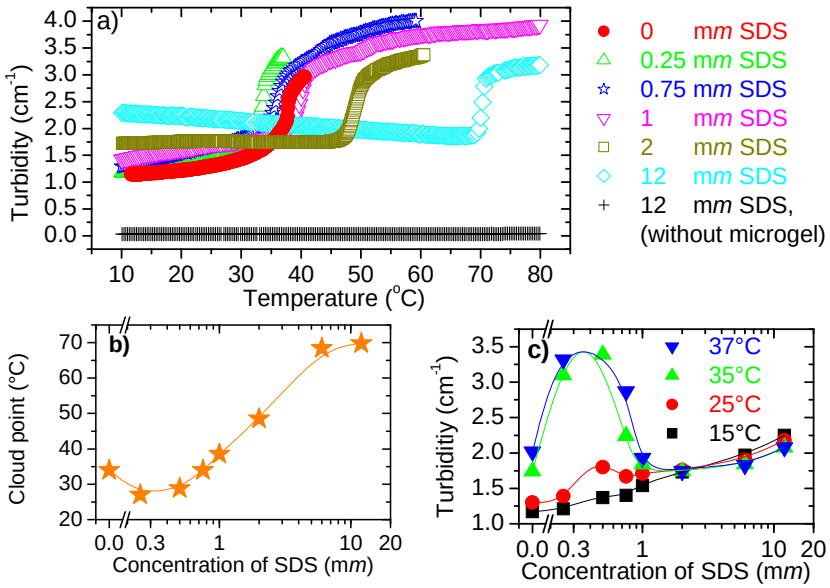

Figure 35: a) *Temperature dependences of the turbidity for an aqueous suspension (0.04 wt %) of uncharged PNIPAAM microgels without SDS and with different concentrations of SDS at pH = 7. b) Plot of cloud point as a function of surfactant concentration for the same system. c) Concentration dependences of turbidity at temperatures indicated.*

IV.2.3.2 Dynamic Light Scattering

The temperature dependence of the hydrodynamic radius is depicted in Figure 36a for various surfactant concentrations. At low surfactant concentrations, the microgels exhibit a similar behavior as was observed in the absences of SDS, i.e., a shrinking of the microgels at low temperatures followed by a raise in R_h caused by aggregation. At higher SDS concentrations, the PNIPAAM microgels contract from approximately 550 nm at 10 °C to 150 nm at about 55 °C, and at higher temperatures the value of R_h is virtually unaffected by temperature. This observation discloses that over the studied temperature domain, the microgels collapse and no growth of aggregates is detected at high temperatures because the particles are decorated by SDS molecules, which generate electrostatic repulsive forces and thereby stabilize the particles against aggregation. It is possible that some of the hydrophobic stickers are solubilized, and this may lead to reduced stickiness of the particles. For the microgel suspension containing 0.75 m*m* SDS, the correlation functions could not be analyzed at temperatures above 40 °C, even though the phase separation does not occur until 58 °C. This problem is probably due to multiple scattering caused by big aggregates formed at elevated temperatures. A similar behavior is detected for microgels with 12 m*m* SDS, even though macroscopic phase separation does not occur at high temperatures for this sample. This might be caused by the formation of a few large aggregates in the suspension.

Again, the temperature-induced compaction of the microgels is accompanied by a strong increase of τ. This feature can be explained in a framework similar to that described above, namely that compression of the species lead to a situation where the relative refractive index of the particles is increased and this leads to higher values of Q_{ext}.

In Figure 36b, the hydrodynamic radius is plotted as a function of the SDS concentration at different temperatures. At low temperatures, the R_h increases as more SDS is added. This is probably due to an expansion of the molecules caused by a SDS-induced

soulibilization of the hydrophobic interactions in the microgels, this is in a good agreement with the data from turbidity.

At elevated temperatures, there is an abrupt drop in R_h between 0.5 and 0.75 mmolal SDS, followed by a slight increase. The drop in R_h indicates the transition between the samples that have a CP below 37 °C, and those that phase separates at higher temperatures. And the following increase is due to the SDS-induced expansion of the microgels.

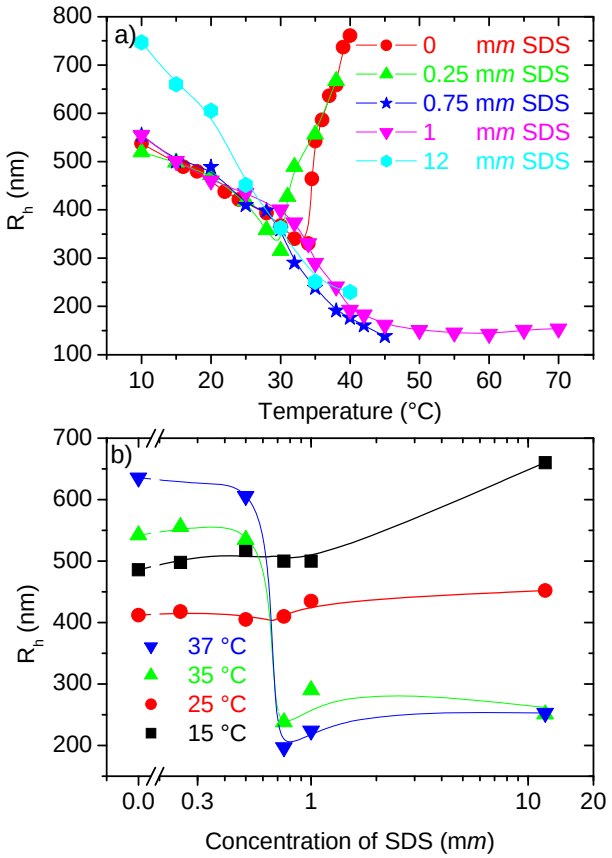

Figure 36: a) *Temperature dependences of the hydrodynamic radius for an aqueous suspension (0.04 wt %) of uncharged PNIPAAM microgels at pH = 7, and at the SDS concentrations indicated. b) Concentration dependences of hydrodynamic radius at temperatures indicated.*

To illustrate the relative change of the apparent hydrodynamic radius with temperature for the different microgels at pH = 7, the ratio R_h/R_h^{10} (R_h^{10} is the hydrodynamic radius at a temperature of 10 ^oC) is plotted in Figure 37. This illustration divulges that up to the LCST, the compression of the particles is more prominent for the systems of low charge density because when the number of charges is high, the charges inside the microgels will give rise to repulsive forces that counteract the intrachain contraction. At higher temperatures, the microgels of systems with higher charge density are decorated with charges onto the surfaces, and this provides the stability of the suspension. It is interesting to note that the samples with 6 mol % AA exhibit exactly the same trend even though the size of the particles differs with a factor of two.

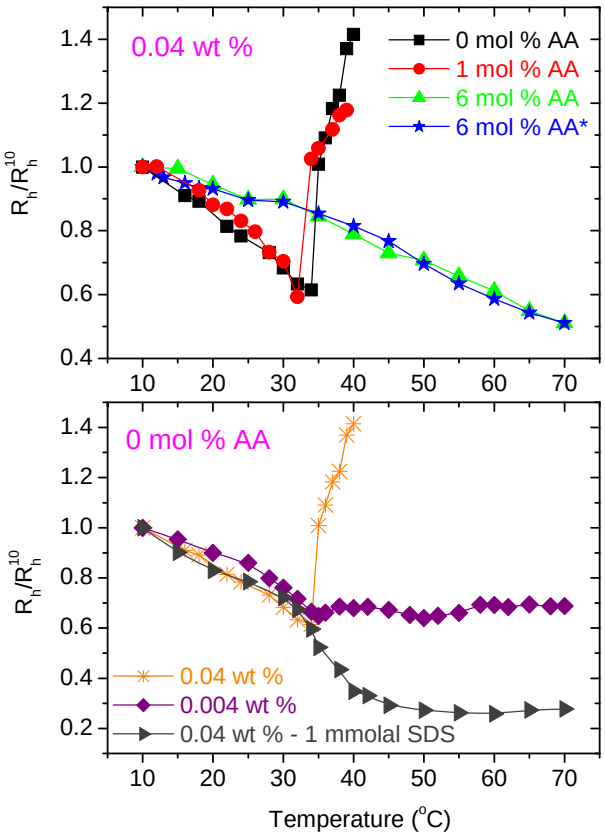

Figure 37: *Temperature dependences of the relative hydrodynamic radius for the systems indicated at pH = 7. The asterisk (6-mol% AA*) in the inset denotes the sample that has been synthesized in the presence of SDS.*

To investigate the kinetics of the restructuring process of the microgels, temperature-quenching experiments were conducted, and the effect of a rapid temperature jump from 32 °C to 37 °C was monitored. Figure 38 illustrates the time evolution of the scattered intensity for some different microgels. The general picture that emerges is that the reorganization of the structures is a fast process at all microgels, and after about 5 min the growth of species has ceased.

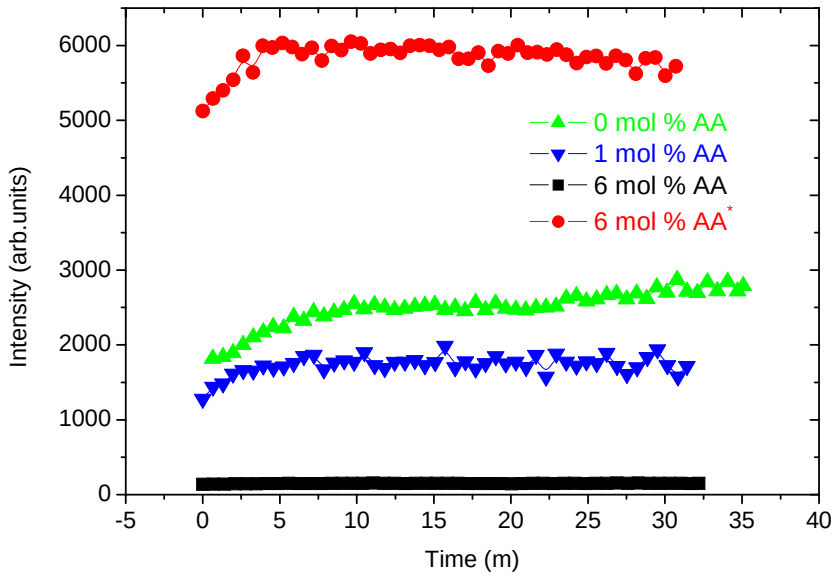

Figure 38: *Time evolution of the reduced scattered intensity at a scattering angle of 90° for 0.04 wt % suspensions of the uncharged PNIPAAM and the charged PNIPAAM-co-PAA microgels at pH=7, when the solutions are exposed to a rapid temperature change (temperature-quenching) from 32 °C to 37 °C. The asterisk (6-mol% AA*) in the inset denotes the sample that has been synthesized in the presence of SDS.*

In order to test the stability of the microgels at elevated temperatures, the correlation functions were collected before and after the heating cycle, and the results are displayed in Figure 39. The normalized correlation function as a function of microgels measured at 25 °C before and after the heating cycle collapsed onto each other. This indicates that the temperature changes are reversible for all microgel systems.

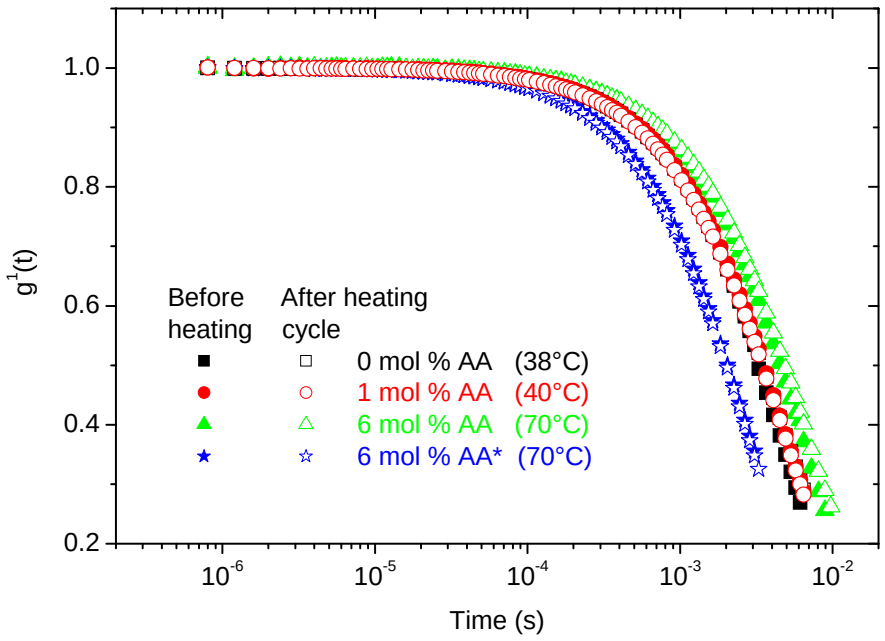

Figure 39: *Plot of the first-order electric field correlation functions versus time at a scattering angle of 90 ° for 0.04 wt% suspensions of the system indicated. All measurements are carried out at 25 °C, the solid symbols are measured before the samples were heated up, and the open symbols are measured after the samples were heated up to the indicated temperatures, and then cooled down again. The asterisk (6-mol% AA*) in the inset denotes the sample that has been synthesized in the presence of SDS.*

V. CONCLUSIONS

In the present work, dilute HEC solutions have been chemically cross-linked at alkaline conditions under the influence of different stirring speeds; at various stages during the cross-linking process the reaction was terminated by quenching the mixture to an acid pH. The results demonstrate that cross-linked particles are produced with a broad size distribution. In the course of cross-linking of polymer chains in the dilute concentration regime, competition between intrachain and interchain cross-linking is an omnipresent phenomenon. It has been shown that when dilute HEC solutions are exposed to high stirring speeds during the cross-linking process, the growth of large aggregates is suppressed. The results from AFFFF sustain this finding and it is also found that the molecular weight and polydispersity of the species is less at high stirring speeds.

It is observed from the DLS measurements that high stirring speeds at early states of the cross-linker reaction promote intrapolymer cross-linking, with contraction of polymer species, and reduction of the growth of aggregates at long reaction times. The sizes of the particles are virtually not affected by temperature in the interval 25-60 ^{o}C.

The results from the rheo-SALS experiments disclosed that at early times during the cross-linker reaction, the complexes are fragile against shear forces if the reaction mixture had been subjected to low stirring speeds. However, high stirring speeds of the reaction mixture in the course of the cross-linking process generates stronger aggregates due to a more efficient packing of the chains in the complexes. At a later state of cross-linking, more cross-links lead to better stability of the species even for solutions that have been exposed to low stirring speeds during the cross-linking process. This work has demonstrated that particles of various sizes can be prepared by exposing the solutions to different stirring speeds during the cross-linker reaction, and to terminate the reaction at desired reaction times. This open the possibility to prepare particles that can be used for enhanced oil recovery applications.

Chemically cross-linked PNIPAAM microgels, and charged analogous PNIPAAM-*co*-PAA microgels were prepared, and the effect of temperatures and pH were scrutinized with the aid of dynamic light scattering and turbidimetry. At temperatures up to the LCST all the studied microgels were observed to shrink, independent of polymer concentration, pH, and charge density. However, the relative contraction is larger for the cross-linked particles with no or low charge density. This significant collapse of the species cannot be traced to a decrease in the turbidity, but rather the value of τ raises. This irregular phenomenon is analyzed in the framework of an approach that takes into account changes of the refractive index of the particles in connection with particle compression. At low temperatures, the size of the microgels with 6 mol-% AA groups is appreciably larger that that of the uncharged particles because of repulsive interactions. However, the microgels with 6 mol-% AA groups that have been synthesized in the presence of SDS are much smaller than all the other microgels.

At temperatures above the LCST, the microgels with one or few charges aggregate, whereas at very low concentrations this tendency of forming flocks is suppressed. The interchain association occurrence is strongly inhibited when a sufficient amount of SDS is added to the uncharged microgels. At pH = 2, all systems approach macroscopic phase separation at temperatures above the LCST. At pH = 7 and pH = 11, most of the features are similar and the results for the charged microgels (6 mol-% AA) demonstrate that the apparent hydrodynamic radius drops continuously over the whole considered temperature range. This finding shows that the microgels are electrostatically stabilized.

Effects of polymer concentration, pH, and charge density on the temperature-induced association behavior of these microgels are schematically illustrated in Figure 40 a,b. The illustration shows that contraction always happens at temperatures below the LCST. We note that at temperatures above the LCST, the uncharged or slightly charged microgels form aggregates, except at very low concentrations or in the presence of SDS. Intuitively, we

would expect that when big aggregates are formed at elevated temperatures for a sample containing many microgel particles, species of various sizes should exist in the suspension. However, values of the stretched exponential β close to 1 at this stage, suggests that the size distribution is narrow. To obtain more information about the species, we have carried out a few cryogenic transmission electron microscopy (cryo-TEM) measurements on 0.04 wt % of uncharged PNIPAAM microgels at a temperature of 38 ^{o}C (large aggregates ($R_h \approx 650$ nm) are formed). The experimental technique and the instrumentation have been described elsewhere [133], as well as the performance of the measurements [98]. The results demonstrate that huge spherical particles with a narrow size distribution are formed see Figure 40c. This finding supports the DLS results that the species are nearly monodisperse, even when phase separation is approached. The diffuse outer rims of the particles in Figure 40c indicate that uniform loosely aggregated species are formed. This finding indicates that the shells are quite tightly bound to the core particles [134].

For suspensions of the charged PNIPAAM-*co*-PAA microgels, the contraction of the particles continues over the entire temperature region at pH = 7 and pH = 11, whereas at pH = 2 large clusters are formed above the LCST and macroscopic phase separation is approached.

For further studies, it can be interesting to investigate the possibility of producing microgels that are stable for long periods of time against very high temperatures (> 90 °C), high pressure, and salinity for the use in EOR applications.

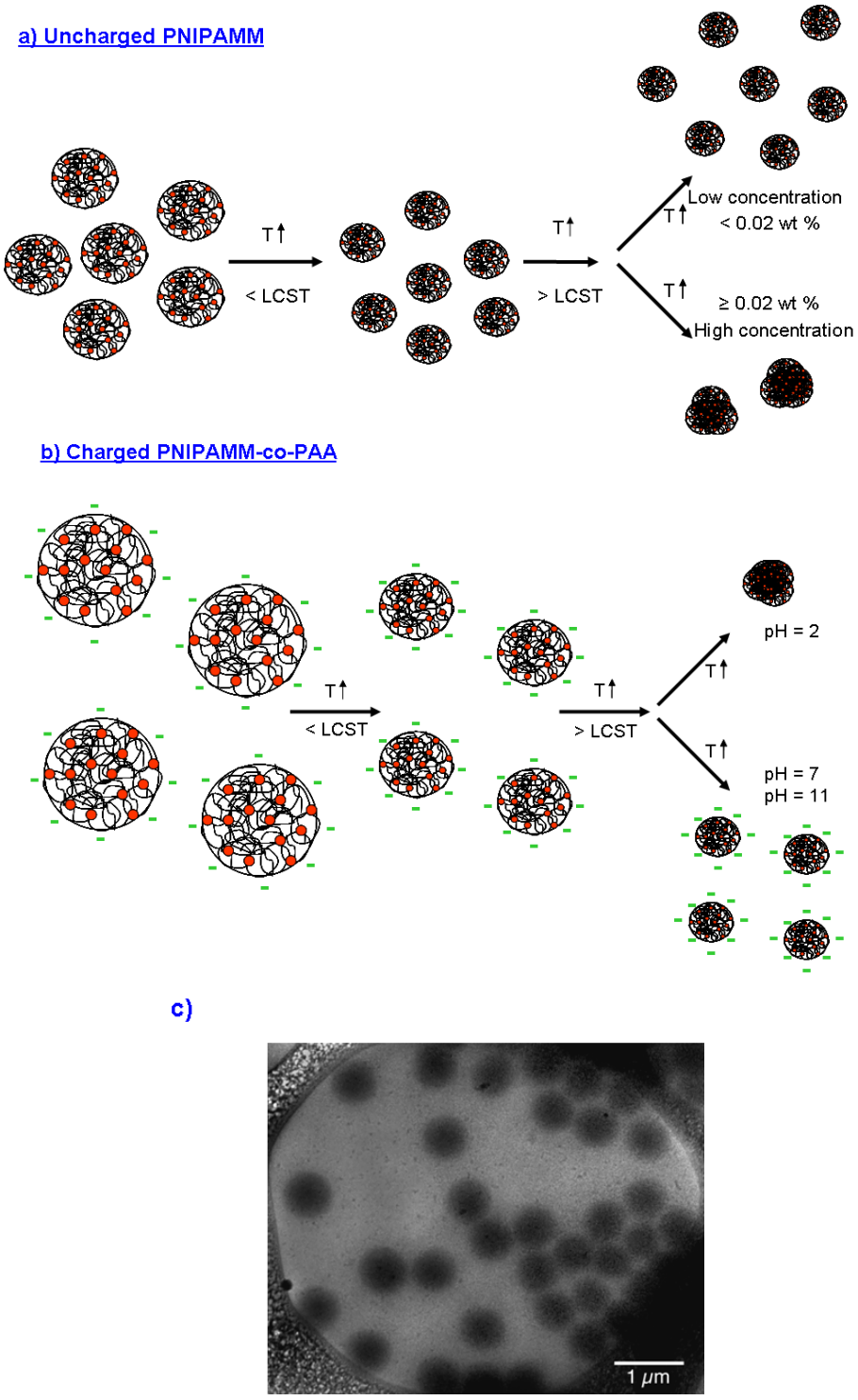

Figure 40: *a) Schematic illustration of effects of polymer concentration for uncharged PNIPAAM on the temperature-induced aggregation behavior of microgels. b) Effects of pH, and charge density for charged PNIPAAM-co-PAA on the temperature-induced aggregation behavior of microgels. The addition of SDS on uncharged particles will give a similar effect as sketched for the charged particles. c) Cryo-TEM image of a 0.04 wt % suspension of uncharged PNIPAAM microgels at 38 °C. The scale bar is 1 μm.*

VI. REFERENCES

1. Deffeyes, K. S., Hubbert`s Peak: The Impending Word Oil Shortage, New Jersey, Princeton University Press **2001**.
2. Reynold, D. B., Scarcity and Growth Considering Oil and Energy, An Alternative Neo-Classical View, Lewiston, N.Y., Edwin Mellen Press **2002**.
3. Mohanty, K. K., The near-term energy challenge. *AIChE J*. **2003**, 49, 2454-2460.
4. Hirsch, R. L.; Bezdek, R.; Wendling, R., Peaking of world Oil Technology Laboratory, U.S. Department of Energy **2005**.
5. Thomas, S.; Farouq-Ali, S. M., *Energy Sources* **1999**, 21, 177.
6. Taber, J. J.; Martin, F. D.; Seright, R. S., *SPE Reservoir Eng.* **1997**, 12, 189.
7. Lake, L. W., Enhanced Oil Recovery. Englewood Cliffs, N.J., Prentice Hall **1989**.
8. Prud`homme, R. K.; Uhl, J. T.; Poinsatte, J. P.; Halverson, F., *Society of Petroleum Eng. J.* **1983**, 23, 804.
9. Maxcy, T. A.; Willhite, G. P.; Green, D. W., *J. of Petroleum Sci. Eng.* **1998**, 19, 253.
10. Vargas-Vasquez, S. M.; Romero-Zerón, L. B., *Petroleum Sci. and Technology* **2008**, 26, 481.
11. Grattoni, C. A.; Al-Sharji, H. H.; Yang, C.; Muggeridge, A. H.; Zimmerman, R. W., *J. Coll. and Interface Sci.* **2001**, 240, 601.
12. Vossoughi, S., *Journal of Petroleum Sci. and Eng.* **2000**, 26, 199.
13. Moradi-Araghi, A., *Journal of Petroleum Sci. and Eng.* **2000**, 26, 1.
14. Chauveteau, G.; Tabary, R.; Renard, M.; Omari, A., *Proceedings – SPE International Symposium on Oilfield Chemistry* **1999**, 507.
15. Wang, W.; Liu,Y.; Gu,Y., *Colloid Polym. Sci* **2003**, 281, 1046.
16. Sun, M.; Ng, W.; Barron, A. E., *Polymeric Materials, sci. and Eng.* **2007**, 96, 115.
17. Kong, B.L.; Han, J., *Shiyou Kantan Yu Kaifa* **2001**, 28, 71. (Abstract).

18. Cowie, J.M.G., Polymer: Chemistry & Physics of Moderen Materials, 2 nd edition, N. W., CRC Press **2000**.

19. Martin Malmsten, Surfactants and Polymers in Drug Delivery, drugs and the pharmaceutical sciences, Marcel Dekker, N.Y., Vol. 112, **2002**.

20. Experimental Methods in Polymer Science, Modern Methods in Polymer Research and Technology, Edited by Tanaka T., Academic Press, USA **2000**.

21. Yeomans, K., *Chem. Rev*. **2000**, 10, 2.

22. Hoffman, A. S., *Adv. Drug Deliv. Rev.* **2002**, 54, 3.

23. Gehrke, S. H., *Advances in Polymer Science* **1993**, 110, 81.

24. Bohidar, H. B., *Curr. Sci*. **2001**, 80, 1008.

25. Sjöström, J. Surfactant responsive cross-linked polymer hydrogels: The history of cross-linked polymer gels, Ph.D. Dissertation, Lund University, Lund, Sweden **2002**.

26. Song, H.; Zhang, S.-F.; Ma, X.-C.; Wang, D.-Z.; Yang, J.-Z., *Carbohydrate Polymers* **2007**, 69, 189.

27. Ali, E.; Ibrahim, V.-F.; Mohammad, I., *Eur. Polym. J.* **2007**, 43, 1986.

28. Pourjavadi, A.; Harzandi, A. M.; Hosseinzadeh, H., *Eur. Polym. J.* **2004**, 40, 1363.

29. Mahdavinia, G. R.; Zohurian-Mehr, M. J.; Pourjavadi, A., *Polym. Adv. Technol.* **2004**, 15, 173.

30. Albonico, P.; Burrafato, G.; Lockhart, T. P., *J. Polym. Sci. Part A: Polym. Chem.* **1992**, 30, 1071.

31. Hennink, W. E.; van Nostrum, *C. F. Adv. Drug Deliv. Rev.* **2002**, 54, 13.

32. Paul S. Russo, Reversible Polymeric Gels and Related Systems, American Chemical Society, Washington, DC **1987**.

33. Eagland, D.; Crowther, N. J.; Butler, C. J., *Eur. Polym. J.* **1994**, 30, 767.

34. Mathur, A. M.; Hammonds, K. F.; Klier, J.; Scranton, A. B., *J. Controlled Release* **1998**, 54, 177.

35. Nyström, B.; Kjøniksen, A.-L.; Lindman, B., *Langmuir*, **1996**, 12, 3233.

36. Kjøniksen, A.-L.; Nyström, B.; Lindman, B., *Macromolecules*,**1998**, 31, 1852.

37. Maleki, A.; Kjøniksen, A.-L.; Nyström, B., *J. Phys. Chem. B* **2005**, 109, 12329.

38. Liu, Z.; Maleki, A.; Zhu, K.; Kjøniksen, A.-L.; Nyström, B., *Journal of Physical Chemistry B*, **2008**, 112(4), 1082.

39. Al-Manasir, N.; Kjøniksen, A.-L.; Nyström, B., *Journal of Applied Polymer Science* In press **2009**.

40. Pelton, R., *Adv. Colloid and Interface Sci.* **2000**, 85, 1.

41. Kawaguchi, H., P*rog. Polym. Sci.* **2000**, 25, 1171.

42. Jeong, B.; Bae, Y. H.; Lee, D. S.; Kim, S. W., *Nature* **1997**, 388, 860.

43. Kurisawa, M.; Terano, M.; Yui, N., *Macromol. Rapid Commun.* **1995**, 16, 663.

44. Brondsted, H.; Kopecek, J., *Pharm. Res.* **1992**, 9, 1540.

45. Miyata, T.; Asami, N.; Uragami, T., *Nature* **1999**, 399, 766.

46. Holtz, J. H.; Asher, S. A., *Nature* **1997**, 389, 829.

47. Umeno, D.; Kawasaki, M.; Maeda, M., *Bioconj. Chem.* **1998**, 9, 719.

48. Kawaguchi, H.; Fujimoto, K., *Bioseparation* **1999**, 7, 253.

49. Bergbreiter, D. E.; Case, B. L.; Liu, Y.-S.; Caraway, J. W., *Macromolecules* **1998**, 31, 6053.

50. Bergbreiter, D. E.; Liu, Y.-S.; Osburn, P. L., *J. Am. Chem. Soc.* **1998**, 120, 4250.

51. Jones, C. D.; Serpe, M. J.; Schroeder, L.; Lyon, L. A., *J. Am. Chem. Soc.* **2003**, 125, 5292.

52. Jones, C. D.; Lyon, L. A., *Macromolecules* **2003**, 36, 1988.

53. Wei, W.; Yuzhang, L.; Yongan, G., *Colloid Polym. Sci.* **2003**, 281, 1046.

54. Braun, O.; Selb, J.; Candau, F., *Polymer* **2001**, 42, 8499.

55. Dowding, P. J.; Vincent, B.; Williams, E., *J. Colloid Interf. Sci.* **2000**, 221, 268.

56. Hernandez, B. J.; Hunkeler, D., *Polymer* **1997**, 38, 5623.

57. Landfester, K.; Willert, M.; Antonietti, M., *Macromolecules* **2000**, 33, 2370.

58. Ming, W. H.; Zhao, Y. Q.; Cui, J.; Fu, S. K.; Jones, F. N., *Macromolecules* **1999**, 32, 528.

59. Neyret, S.; Vincent, B., *Polymer* **1997**, 38, 6129.

60. Platkowski, K.; Pross, A.; Reichert, K. H., *Polym. Int.* **1998**, 45, 229.

61. Pross, A.; Platkowski, K.; Reichert, K. H., *Polym. Int.* **1998**, 45, 22.

62. Al-Manasir, N.; Zhu, K.; Kjøniksen, A.-L.; Knudsen, K. D.; Karlsson, G.; Nyström, B., Submitted to *J. Phys. Chem. B* **2009**.

63. Kjøniksen, A.-L.; Nyström, B.; Lindman, B., *Langmuir* **1998**, 14, 5039.

64. Kjøniksen, A.-L.; Nyström, B.; Lindman, B., *Colloids and Surface A* **1999**, 149, 347.

65. Kwak, J. C. T., Polymer-surfactant Systems, Marcel Dekker, New York, Vol. 77 **1998**

66. Tanaka, R.; Meadows, J.; Williams, P. A.; Phillips, G. O., *Macromolecules* **1992**, 25, 1304.

67. Thuresson, K.; Nilsson, S.; Lindman, B., *Langmuir* **1996**, 12, 2412.

68. Nilsson, S.; Thuresson, K.; Hansson, P.; Lindman, B., *J. Phys. Chem. B* **1998**, 102, 7099.

69. Lauten, R. A., Solution and interface characteristics of two water-soluble amiphiphilic polymer systems. Ph.D. Dissertation, University of Oslo **2004.**

70. Lund, R.; Lauten, R. A.; Nyström, B.; Lindman, B., *Langmuir* **2001**, 17, 8001.

71. Lauten, R. A.; Nyström, B., *Colloids and Surf. A* **2003**, 219, 45.

72. Lauten, R. A.; Kjøniksen, A.-L.; Nyström, B., *Langmuir* **2000**, 16, 4478.

73. Beheshti, N., Master's Degree in Chemistry, Department of Chemistry, Faculty of Mathematics and Natural Sciences, University of Oslo, Oslo, **2006**.

74. Wiley, J. and Sons, *Encyclopedia of Chemical Technology* **1991**, 5.

75. Marci, G.; Mele, G.; Palmisano, L.; Pulito, P.; Sannino, A., *Green Chemistry* **2006**, 8, 439.

76. Lu, X.; Hu, Z.; Gao, J., *Macromolecules* **2000**, 33, 8698.

77. Hu, Z.; Lu, X.; Gao, J., *Adv. Mater.* **2001**, 13,1708.

78. Liu, S.; Weaver, J.V.M.; Save, M.; Armes, S.P., *Langmuir* **2002**, 18, 8350.

79. White, M. L.; Dorion, G. H., *J. Polym. Sci.* **1961**, 55, 731.

80. White, M. L., *J. Phys. Chem.* **1963**, 64, 1563.

81. Hirokawa, Y.; Tanaka, T.; Matsuo, E. S., *J. Chem. Phys.* **1984**, 81, 6379.

82. Yang, Y., Synthesis and characterization of hydrophobically modified polyacrylamide-based polymers, Ph.D. Dissertation, University of New York, New York, NY **1996**.

83. Fevola, M. J., Model polyzwitterions on polyacrylamide: Synthesis, characterization, and stimuli-responsive solution behavior in aqueous media, Ph.D. Dissertation, University of Southern Mississippi, Hattiesburg, MS **2003**.

84. Hoare, T.; Pelton, R., *Macromolecules* **2004**, 37, 2544.

85. Amalvy, J. I.; Wanless, E. J.; Li, Y.; Michailidou, V.; Armes, S. P., *Langmuir* **2004**, 20, 8992.

86. Neyret, S.; Vincent, B., *Polymer* **1997**, 38, 6129.

87. Kaneda, I.; Vincent, B., *J. Colloid Interface Sci.* **2004**, 274, 49.

88. Fernandez-Nieves, A.; Marquez, M., *J. Chem. Phys.* **2005**, 122, 84702.

89. Schild, H. G., *Prog. Polym. Sci.* **1992**, 17, 163.

90. Karsa, D. R., Surfactants in Polymers, Coatings, Inks, and Adhesives, CRC Press LLC **2003**.

91. Holmberg, K., Novel Surfactants: Preparation, Applications, and Biodegradability, surfactant science series, Vol. 114, 2 nd edition, CRC Press **2003**.

92. Mukerjee, P.; Mysels, K. J., Critical Micelle Concentration of Aqueous Surfactant Systems, NSRDS-NBS 36, U.S. Government Printing Office, Washington, D.C., **1971.**

93. Egemayer, M.; Norman, J.; Picullell, L., *Langmuir* **2003**, 19, 10036.

94. Baglioni, P.; Dei, L.; Ferroni, E.; Kevan, L., *Prog. Colloid Polym. Sci.* **1991**, 84, 55.

95. Abuin, E. B.; Lissi, E. A.; Borsarelli, C., *J. Colloid Interface Sci.* **1996**, 184, 652.

96. Kjøniksen, A-L.; Zhu, K.; Pamies, R.; Nyström, B., *J. Phys. Chem. B* **2008**, 112, 3294.

97. Pamies, R.; Zhu, K.; Kjøniksen, A-L.; Knudsen, K. D.; Nyström, B., *J. Colloid Interface Sci.* **2008**, 326, 76.

98. Kjøniksen, A-L.; Zhu, K.; Karlsson, G.; Nyström, B., *Colloid and Surfaces A: Physicochem. Eng. Aspects* **2009**, 333, 32.

99. Siegert, A. J. F. Massachusetts Institute of Technology, Radiation Laboratory Report no. 465, 1943.

100. Kohlrausch, R. *Prg. Ann. Phys.* **1847**, *12*, 393.

101. Williams, G.; Watts, D. C. *Trans. Faraday Soc.* **1970**, *66*, 80.

102. Nagi, K. L., *Adv. Colloid Interface Sci.* **1996**, 64, 1.

103. Phillies, G. D. J.; Richardson, C.; Quinlan, C. A.; Ren, S Z. *Macromolecules* **1993**, 26, 6849.

104. Phillies, G. D. J.; Lacroix, M. *J. Phys. Chem. B* **1997**, *101*, 39.

105. Kjøniksen, A.-L.; Joabsson, F.; Thuresson, K.; Nyström, B. *J. Phys. Chem. B* **1999**, 103, 9818.

106. Kjøniksen, A-L.; Nyström, B.; Lindman, B., *Langmuir* **1998**, 14, 5039.

107. Lauten, R. A.; Nyström, B., *Collods Surf. A* **2003**, 219, 45.

108. Yan, X.; Xu, X.; Zhu, L., *J Mater Sci* **2007**, 42, 8645.

109. Fraunhofer, W.; Winter, G., *Eur. J. of Pharm. And Biopharm*. **2004**, 58, 369.

110. Leeman, M.; Islam, M. T.; Haseltine, W. G., *J. of Chromatography A* **2007**, 1172, 194.

111. Augsten, C.; Maeder, K., *International Journal of Pharmaceutics* **2008**, 351, 23.

112. Lee, H.; Cho, I.-H.; Moon, M. H., *Journal of Chromatography A* **2006**, 1131, 185.

113. Alasonati, E.; Benincasa, M.-A.; Slaveykova, V.I., *Journal of Separation Science* **2007**, 30, 2332.

114. Jones, C. D.; Lyon, L. A., *Macromolecules* **2000**, *33*, 8301.

115. Pelton, R. *Adv. Colloid Interface Sci*. **2000**, *85*, 1.

116. Anderson, M.; Maunu, S. L. *J. Polym. Sci. Part B: Polym. Phys*. **2006**, *44*, 3305.

117. Zhu, K.; Jin, H.; Kjøniksen, A.-L.; Nyström, B., *J Phys Chem B* **2007**, 111, 10862.

118. Kjøniksen, A.-L.; Nyström, B., *Macromolecules* **1996**, 29, 7116.

119. Nyström, B.; Walderhaug, H.; Hansen, F. K., *J. of Physical Chemistry* **1993**, 97, 7743.

120. Sun, Z.; Wang, C. H., *Macromolecules* **1994**, 27, 5667.

121. Martin, J.; Wilcoxon, J. P., *Physical Review Letters* **1988**, 61, 373.

122. Snowden, M. J.; Chowdhry, B. Z., Vincent, B.; Morris, G. E. *J. Chem. Soc., Faraday Trans.* **1996**, *92*, 5013.

123. Saunder, R. S.; Vincent, B., *Adv. Colloid Interface Sci.* **1999**, 80, 1.

124. Tan, B. H.; Tam, K. C. *Adv. Colloid Interface Sci.* **2008**, *136*, 25.

125. Heller, W.; Pangonis, W. J. *J. Chem. Phys*. **1957**, *26*, 498.

126. Lechner, M. D. *J. Serb. Chem. Soc.* **2005**, *70*, 361.

127. Winnik, F. M., *Macromolecules* **1990**, 23, 233.

128. Wu, C.; Zhou, S. *Macromolecules* **1995**, *28*, 8381.

129. Wu, C.; Wang, X. *Phys. Rev. Lett.* **1998**, *80*, 4092.

130. Wang, X.; Qui, X.; Wu, C. *Macromolecules* **1998**, *31*, 2972.

131. Jean, B.; Lee, L.-T.; Cabane, B. *Colloid Polym. Sci*. **2000**, *278*, 764.

132. Kjøniksen, A.-L.; Hiort, M.; Nyström, B., *European Polymer Journal* **2005**, 41, 761.

133. Almgren, M.; Edwards, K.; Karlsson, G. *Colloid Surf. A* **2000**, *174*, 3.

134. Crassous, J. J.; Ballauf, M.; Drechsler, M. ; Schmidt, J.; Talmon, Y., *Langmuir* **2006**, 22, 2403.